BULGARIAN ACADEMY OF SCIENCES

INSTITUTE OF ORGANIC CHEMISTRY WITH CENTRE OF PHYTOCHEMISTRY

Laboratory "Structural Organic Analysis"

A B S T R A C T

For awarding the **Doctor** degree

Professional area 4.2 "Chemical Sciences"

Specialty: "Organic chemistry"

Synthesis of 1*H*-benzimidazol-2-yl hydrazones and study of their anthelmintic, antineoplastic and radical scavenging activities

Maria Andreeva Argirova

Supervisor: Prof. Dr. Denitsa Pantaleeva

Sofia, 2023

The dissertation contains 219 pages, 56 figures, 20 tables and 69 schemes. The bibliography contains 293 literature sources.

The dissertation was discussed and proposed for defense of a meeting of the Colloquim on “Finctional materials, computional modeling and technologies” at the Institute of Organic Chemistry with Centre of Phytochemistry – BAS with Protocol № 48 on 30.11.2022.

The studies in the dissertation were carried out in the laboratory "Structural Organic Analysis" at the IOHTCF-BAS; Department of Chemistry at New University of Lisbon - Portugal, Faculty of Pharmacy and Faculty of Medicine at Medical University - Sofia; Department of Infectious Diseases, Parasitology and Tropical Medicine, Medical University - Plovdiv.

The thesis defense will be held on …… at ……. in ….....…..

Scientific jury:

1. Prof. Antoaneta Trendafilova, PhD, IOCCP, BAS
2. Assoc. Prof. Snezhana Bakalova, PhD, IOCCP, BAS
3. Prof. Dsc. Sonia Ilieva, Faculty of Chemistry and Pharmacy, Sofia University "St. Kliment Ohridski"
4. Assoc. Prof. Stela Statkova, PhD, Faculty of Chemistry, University of Plovdiv
5. Assoc. Prof. Jivko Velkov, PhD, South-West University "Neofit Rilski"

Reserve Members:

1. Prof. Adriana Bakalova, PhD, Medical university-Sofia
2. Assoc. Prof. Nadezhda Markova, PhD, IOCCP, BAS

The numbering of the figures, schemes and tables in the abstract does not correspond to that used in the dissertation.

I. Introduction

The potential of the benzimidazole fragment for the development of novel pharmacologically active compounds in well known. Many benzimidazoles have found application in the therapeutic practice – nocodazole, bendamustine, denibulin, dovitinib, albendazole, mebendazole etc. 2-Aminobenzimidazole heterocycle is a structural fragment frequently encountered in these drugs and it is of main importance as a precursor for the synthesis of novel benzimidazoles with antitumor and anthelmintic activity.

Some structural derivatives were synthesized – such as 2-aminobenzimidazole Shiff bases, and have shown cytotoxic activity toward several cancer cell lines: SW707 (colorectal carcinoma/rectal adenocarcinoma), HCV29T (bladder cancer), A549 (A549 (non-small cell lung carcinoma), T47D (breast cancer) and PC-3. Other derivatives - N′-(4-arylidene)-1H-benzo[d]imidazole-2-carbohydrazides – derivatives with carbonyl hydrazone fragments at C2 position of the benzimidazole ring, have also shown activity in the low micromolar range against different cell lines such as murine leukemia (L1210), human T-cell leukemia (CEM), human cervix carcinoma (HeLa), human pancreas carcinoma cells (Mia Paca-2). 2-Acetylpyridine hydrazone derivatives of benzothiazole, benzoxazole, and benzimidazole exhibited potent cytotoxic activity against the growth of suspended leukemia and lymphomas and a number of solid tumor cell lines – HeLa, SOS (bone osteosarcoma), MCF-7 (breast cancer), MB9812 and A549 (lung cancer). Among the 2-acetylpyridine hydrazone derivatives of benzimidazole, 1-methylbenzoimidazol-2-yl hydrazone (EPH116) was outlined as very promising due to its potent inhibition of colon carcinoma and melanoma cells.

Oxidative stress is leading to cellular structure damage and indirectly might induce DNA mutations, gene instability and cellular proliferation thus contributing to carcinogenesis. It is known that ROS act as a secondary precursor in the intracellular signaling pathway that induce and maintain the oncogenic phenotype of the cancer cells and at the same time ROS are able to induce aging and apoptosis which contributes to their anti-tumorogenic effect. The increased generation of ROS is characteristic for cancer cells where changes in the signal transduction are observed. The DNA mutations have a key role in carcinogenesis, evidence of which are the increased levels of oxidative DNA changes (8-OH-G). In this regard, the antioxidants might contribute as a useful therapeutic agent in the fight against cancer. The advantages of therapy that combines antineoplastic with antioxidant action are highlighted by the broad studies of melatonin. Due to its antioxidative effect and free radical scavenging properties melatonin could provide protection against damage from carcinogenic substances. On the other hand, it exerts an anticancer activity by inhibiting the proliferation and growth of tumor cells, inducing apoptosis. Having in mind the scientific data related to the oxidative stress and the processes of carcinogenesis, it is of interest to study compounds with antioxidant properties as potential antineoplastic agents.

Combined therapy with antioxidant activity would also have a beneficial effect in the treatment of parasitic infections, which are often results in oxidative stress caused by tissue damage, dysfunction of the immune system, and intoxication from the massive killing of parasites.

Current strategies for developing anticancer drugs focus on targeting various biological targets such as tubulin. A number of tubulin inhibitors are currently approved as chemotherapeutic agents for treating of cancer. On the other hand, many of the antimitotic drugs exhibit undesirable toxicity or drug resistance thus leading to nessecary of development of new drug candidates. It is known from the literature that benzimidazole

derivatives could bind selectively to β-tubulin and inhibit the tubulin polymerization in the parasites.

Based on this, the design and synthesis of new benzimidazole derivatives combining 2-aminobenzimidazole fragment, hydrazone chain and substituted phenyl moiety, exhibiting complementary antioxidant and antineoplastic/anthelmintic activity, is of great interest from a synthetic and pharmacological point of view.

II. Aim and tasks

The present dissertation is focused on the synthesis of new 1*H*-benzimidazol-2-yl hydrazones and study of their anthelmintic, antineoplastic and radical-scavenging activity. The following tasks were defined:

1. Synthesis of 1*H*-benzimidazol-2-yl hydrazones containing phenyl fragments with fluoro-, dioxolylmethylene-, hydroxy- and methoxy-substituents
2. Synthesis of metal complexes of selected 1*H*-benzimidazol-2-yl hydrazones;
3. Study of the molecular structure of the synthesized benzimidazole derivatives and their metal complexes by IR, NMR, Raman spectroscopy, scanning electron microscopy with energy dispersive X-Ray analysis (SEM-EDX), elemental analysis and quantum chemical calculations;
4. Study of the antineoplastic and anthelmintic activity of the synthesized compounds;
5. Study of the effect of the obtained hydrazones on the tubulin polymerization;
6. Study of their radical-scavenging activity in chemical and biologically relevant systems;
7. Study of molecular descriptors, probable mechanisms of antioxidant activity and ligand-receptor interactions by theoretical methods.

III. Results and discussion

1. Synthesis

The introduction of various functional groups was achieved by a multi-step synthesis. The benzimidazole core was modified by implementation of a substituent at 5(6)-position and a hydrazone chain at 2-position with an aromatic fragment containing various combinations of hydroxyl and other groups. The structures of the phenylenediamines were chosen in order to tune the lipophilicity of the target compounds. The hydrazones would possess several pharmacophores in order to interact with biological targets and exhibit the desired biological activities.

1.1. Synthesis of 1H-benzimidazol-2-yl hydrazones

The synthesis of the 1*H*-benzimidazol-2-yl-thiols **2.1** and **2.2** was carried out by refluxing ethanol-water solution of potassium hydroxide, carbon disulphide and o-phenylenediamine:

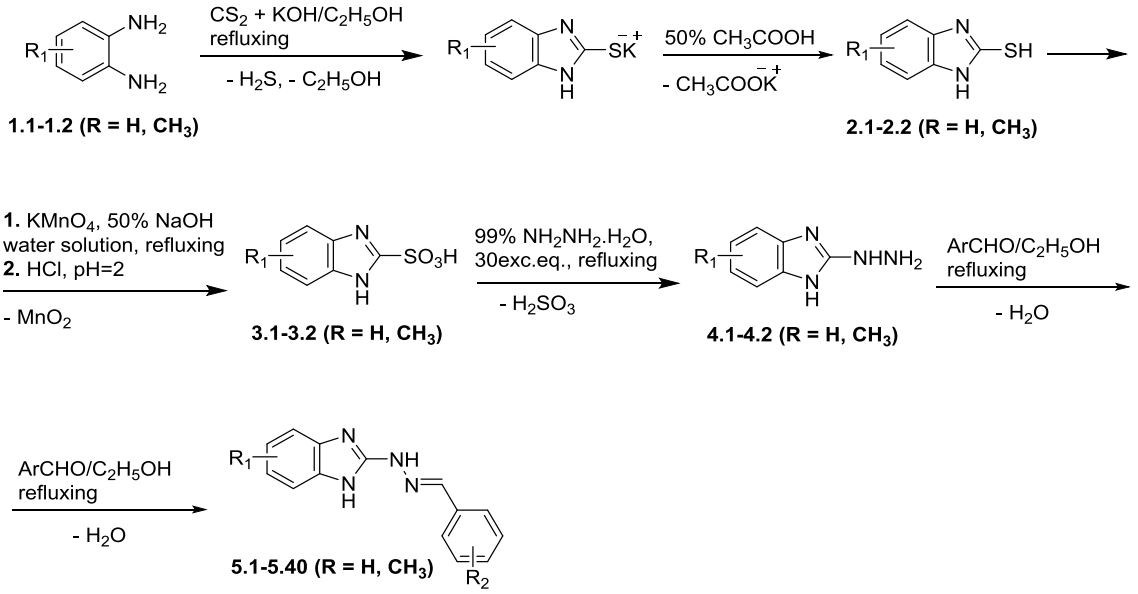

Scheme 1. Synthesis of 1H-benzimidazol-2-yl hydrazones from series A, B and C

1*H*-benzimidazol-2-yl-sulfonic acids **3.1** and **3.2** were obtained by oxidation of 1*H*-benzimidazole-2-thiols **2.1** and **2.2** in a 50 % sodium solution of potassium permanganate for 1 h. The 1*H*-benzimidazol-2-yl-sulfonic acids **3.1** and **3.2** were converted in hydrazines **4.1** and **4.2** by refluxing them for 3 hours in excess of 99% hydrazine hydrate.

The 1*H*-benzimidazol-2-yl hydrazones from series A (Scheme 2) were synthesized through reaction of condensation between 1*H*-benzimidazole-2-yl-hydrazines **4.1** and **4.2** and various hydroxyl-, methoxyl- and fluoro-substituted benzaldehydes, and piperonal in molar ratio 1:1 and using ethanol, 99%, as a solvent.

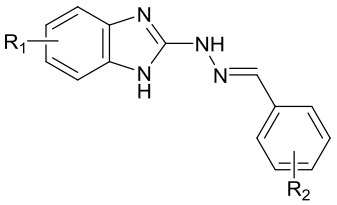

(5.1) R_1=H; R_2= 2-F
(5.2) R_1=H; R_2= 3-F
(5.3) R_1=H; R_2= 4-F
(5.4) R_1=5(6)-CH_3; R_2= 2-F
(5.5) R_1=5(6)-CH_3; R_2= 3-F
(5.6) R_1=5(6)-CH_3; R_2= 4-F
(5.7) R_1=H; R_2= 3,4-OCH_2O-
(5.8) R_1=5(6)-CH_3; R_2= 3,4-OCH_2O-
(5.9) R_1=H; R_2= 3-OH
(5.10) R_1=5(6)-CH_3; R_2= 3-OH
(5.11) R_1=H; R_2= 4-OH
(5.12) R_1=H; R_2= 3-OCH_3
(5.13) R_1=H; R_2= 3-OCH_3-4-OH
(5.14) R_1=5(6)-CH_3; R_2= 3-OCH_3-4-OH
(5.15) R_1=H; R_2= 3,5-diOCH_3-4-OH

Scheme 2. 1H-benzimidazol-2-yl hydrazones from series A

The studies of the biological activities of the 1*H*-benzimidazol-2-yl hydrazones from series A (discussed below) outlined the compounds containing hydroxyl- and methoxyl substituents in the phenyl ring as more promising. This motivated the synthesis of hydrazones from series B (Scheme 3) containing an unsubstituted benzimidazole fragment and benzaldehydes with new combinations of hydroxyl- and methoxyl substituents at different positions:

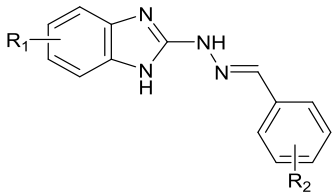

(5.16) R_1=H; R_2= 2-OH
(5.17) R_1=H; R_2= 2,3-diOH
(5.18) R_1=H; R_2= 2,4-diOH
(5.19) R_1=H; R_2= 3,4-diOH
(5.20) R_1=H; R_2 =2,3,4-triOH
(5.21) R_1=H; R_2= 4-OCH_3
(5.22) R_1=H; R_2= 2,6-diOCH_3
(5.23) R_1=H; R_2= 3,5-diOCH_3
(5.24) R_1=H; R_2= 3,4,5-triOCH_3
(5.25) R_1=H; R_2= 2-OH-3-OCH_3
(5.26) R_1=H; R_2= 2-OH-4-OCH_3
(5.27) R_1=H; R_2= 3-OH-4-OCH_3

Scheme 3. 1H-benzimidazol-2-yl hydrazones from series B

As a next step in the structural modification we obtained the hydrazones from series C containing a methyl group in the benzimidazole core at 5(6)-position and hydroxyl- and methoxy substituents in the phenyl moiety (Scheme 4).

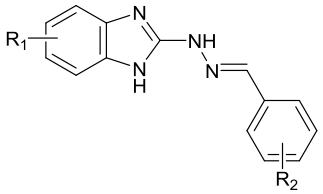

(5.28) R_1=5(6)-CH_3; R_2= 2-OH
(5.29) R_1=5(6)-CH_3; R_2= 2,3-diOH
(5.30) R_1=5(6)-CH_3; R_2= 2,4-diOH
(5.31) R_1=5(6)-CH_3; R_2= 3,4-diOH
(5.32) R_1=5(6)-CH_3; R_2=2,3,4-triOH
(5.33) R_1=5(6)-CH_3; R_2= 4-OCH_3
(5.34) R_1=5(6)-CH_3; R_2= 2,6-diOCH_3
(5.35) R_1=5(6)-CH_3; R_2= 3,5-diOCH_3
(5.36) R_1=5(6)-CH_3; R_2= 3,4,5-triOCH_3
(5.37) R_1=5(6)-CH_3; R_2= 2-OH-3-OCH_3
(5.38) R_1=5(6)-CH_3; R_2= 2-OH-4-OCH_3
(5.39) R_1=5(6)-CH_3; R_2= 3-OH-4-OCH_3
(5.40) R_1=5(6)-CH_3; R_2= 3,5-diOCH_3-4-OH

Scheme 4. 1H-benzimidazol-2-yl hydrazones from series C

Identification of the 1*H*-benzimidazole-2-yl hydrazones was achieved by spectroscopic techniques FT-IR, ^{1}H NMR and ^{13}C NMR. The purity of the compounds was confirmed by thin layer chromatography.

The formation of the azomethine bond was identified by disappearance of the strong doublet for N-H stretching vibration, characteristic for the hydrazines **4.1** and **4.2**, and appearance of a bands for the C=N stretching in the region 1638-1606 cm^{-1} of the IR spectra of the 1*H*-benzimidazole-2-yl hydrazone products. The N-H bonds in the benzimidazolyl fragment and hydrazone moiety gave rise to strong peaks varying within the region 3370-3160 cm^{-1}. The C-O stretching vibrations of the methoxyl groups, were found as intense broad bands around 1265 and 1135 cm^{-1}. In the IR spectra of the compounds containing hydroxyl groups another band for C-O stretching was observed around 1200 cm^{-1}, while the bands of the corresponding O-H stretching vibrations appeared from 3332 to 3468 cm^{-1}.

In the ^{1}H-NMR spectra of the synthesized hydrazones the signals for the protons of the azomethine group were found at 7.9-8.2 ppm as singlets. The benzimidazole protons produced multiplet signals within the interval 6.9-7.4 ppm in DMSO solvent, while the phenyl protons resonated in the interval 6.9-7.8 ppm. The chemical shift values for the protons for the NH and OH protons varied in a broader range – 11.3-11.6 and 9.87-10.95 ppm. A substituent methyl group in the benzimidazole heterocycle gives a singlet at the strong fields - about 3.5-3.7 ppm.

In the ^{13}C NMR spectra, the signals for the azomethine carbon atoms and those at the 2-position in the benzimidazole ring vary in a wider range 127–145 ppm depending on the structure of the compounds. The signals for the aromatic carbon atoms of the phenyl core and the benzimidazole ring were registered between 107 and 135 ppm. The presence of a

methyl group at the 5(6)-position in the benzimidazole fragment gave signals at 21-22 ppm. Signals for carbon atoms bonded to hydroxyl groups were registered between 161 and 145 ppm. The carbon atoms of the methoxy groups resonated at 55-60 ppm.

1.2. Synthesis of metal complexes of the 1H-benzimidazol-2-yl hydrazones

It is known that metal ions, such as iron, are among the main initiators of oxidative damage. These elements easily participate in reactions of complexation and exhibit reducing properties. In their presence, the processes of oxidative damage occur faster and the antioxidants in the human organism are unable to neutralize the free radicals. H_2O_2 in the presence of transition metal ions, through the iron-mediated Fenton reaction, leads to the formation of highly reactive hydroxyl radicals that initiate lipid peroxidation and cell death.

One of the main tasks of this dissertation was the synthesis of metal complexes of some of the newly synthesized 1*H*-benzimidazol-2-yl hydrazones. According to literature data, the synthesis of metal complexes of benzimidazole derivatives could be carried out by two approaches. In both methods, an ethanolic solution of the salt is added to an ethanolic solution of the ligand, and the reaction is conducted by addition of a sodium base (at a pH of the medium in the range of 7.5 to 8.0) or without the addition of a base. In the present work, the synthesis of the complexes was obtained by mixing an ethanolic solution of the salt ($CuCl_2$ or $FeCl_2$) with an ethanolic solution of the corresponding 1*H*-benzimidazol-2-yl hydrazone in a molar ratio 2:1. The reaction mixture was stirred in an ultrasonic bath at 40-50°C for 3-4 hours (Scheme 5).

The structure of the isolated metal complexes was elucidated by IR and micro-Raman spectroscopy, elemental analysis and SEM-EDX. In the IR spectra of the complexes, the bands for the stretching vibrations of the N-H bonds (ν_{N-H}) were observed in the region 3231-3221 cm^{-1}, those for the stretching vibrations of the azomethine bond ($\nu_{C=N}$) – in the region 1607-1599 cm^{-1}, as well as for the stretching vibrations of the C-O bond (ν_{C-O}) – in the region 1508-1491 cm^{-1}.

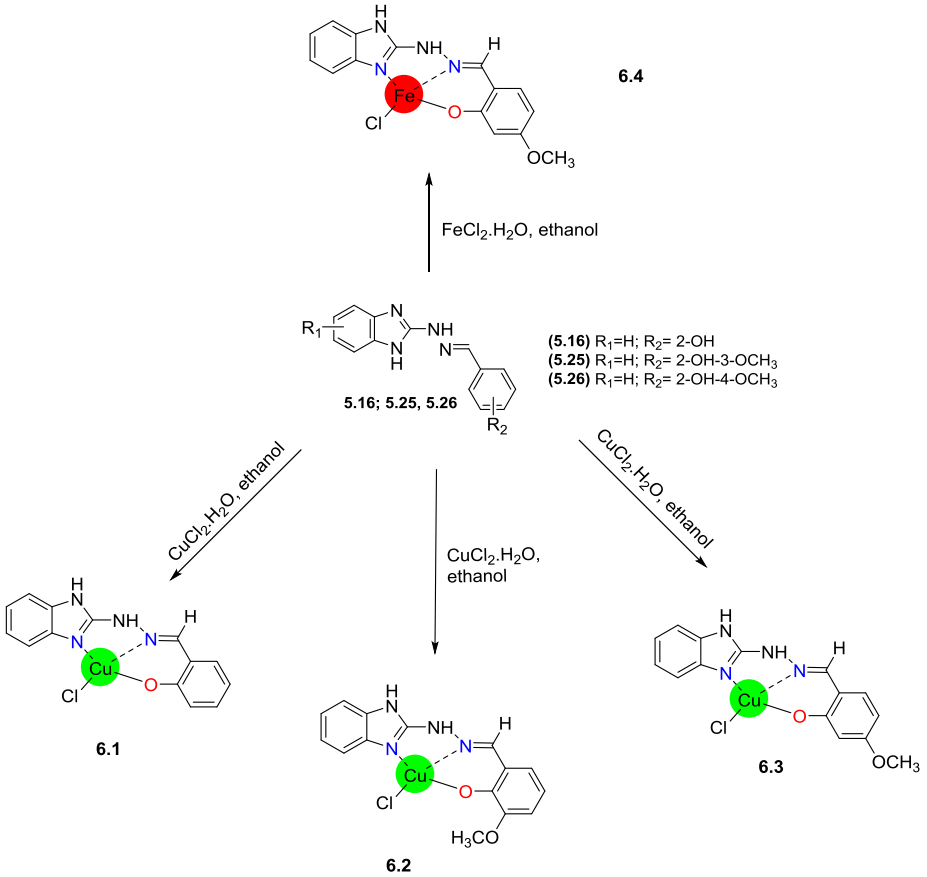

*Scheme 5. Synthesis of metal complexes **6.1-6.4** of the 1H-benzimidazol-2-yl hydrazones*

In the micro-Raman spectra, the bands for the stretching vibrations of the bonds Cu-O and Cu-N (ν_{Cu-O} and ν_{Cu-N}) appeared around 589-587 cm^{-1} and 491-477 cm^{-1}. The results from SEM-EDX analysis showed the presence of the elements Cu and Cl, respectively Fe and Cl, in a ratio of 1:1. Considering also the amount of elements N, C and H established by elemental analysis, it was confirmed that the complexes were formed by coordination of one hydrazone molecule with one metal atom.

2. *Study of the molecular structure by quantum-chemical calculations*

In order to rationalize the observed effects, the molecular structure of the target compounds were characterized by DFT methods. In consideration of the fact that the studied compounds could exist in two tautomeric forms – amino and imino, their geometries were optimized fully using (U)B3LYP density functional theory (DFT) method and 6-311++G** basis set in gas phase and solvents: water and benzene. Solvent effects were included in the optimizations by using the Polarizable Continuum Model (PCM). Single-point (SP) energy calculations were performed additionally at the M062X/6-311+G** level of theory, on the optimized B3LYP geometries. The calculated geometries included also *Z* and *E* configurations of the double C=N (azomethine) bond, *s-cis* and *s-trans* conformation of the N-N bond, and different orientations of the substituents in the phenyl ring for both tautomeric forms. On the other hand, two positional isomers were outlined - at the 5- and 6-position, when considering the presence of a methyl group in the benzimidazole heterocycle.

2.1. Molecular structure of 1H-benzimidazol-2-yl hydrazones containing an unsubstituted benzimidazole moiety

Summarizing the computations, the imino form strongly prevails in all compounds containing hydroxyl group in *ortho* position of the phenyl ring, otherwise the amino form is the favourable one. The energy difference between them is about 2.06-12.88 kJ.mol^{-1}.

The results for two hydrazones, **5.17** and **5.19**, are illustrated below (Figure 1). For compound **5.19** (Figure 1a) containing two hydroxyl groups at positions 3 and 4 in the phenyl ring and showing the most potent radical scavenging effect towards free stable radicals ABTS and DPPH, the amino:imino ratio is: 81.66:18.34 (gas phase); 91.97:8.03 (water); 96.18:3.82 (benzene) according to the B3LYP calculations. The results obtained with SP M06-2X functional indicate even greater prevalence of the amino form in all kind of media: 90.60:9.40 (gas phase); 96.87:3.13 (water); 98.37:1.63 (benzene) respectively.

On the other hands, for compound **5.17** (Figure 1b) containing also two hydroxyl groups, but at positions 2 and 3 in the phenyl ring and showing the highest protection effect towards lecithin and deoxyribose, the amino:imino ratio is 3.48:96.52 (gas phase); 9.98:90.02 (water); 4.60:95.40 (benzene) according to the B3LYP calculations.

The optimized molecular structures of the most stable isomers of compounds **5.17** (in imino tautomeric form) and **5.19** (in amino tautomeric form) are presented for illustration in Figures 4 and 5. The computational results showed that *E* configuration of the double azomethine bond is more stable for both amino or imino form, as well as *s-trans* – for the arrangement around the N-N bond. The molecular geometry of the preferred amino and imino isomers is essentially flat.

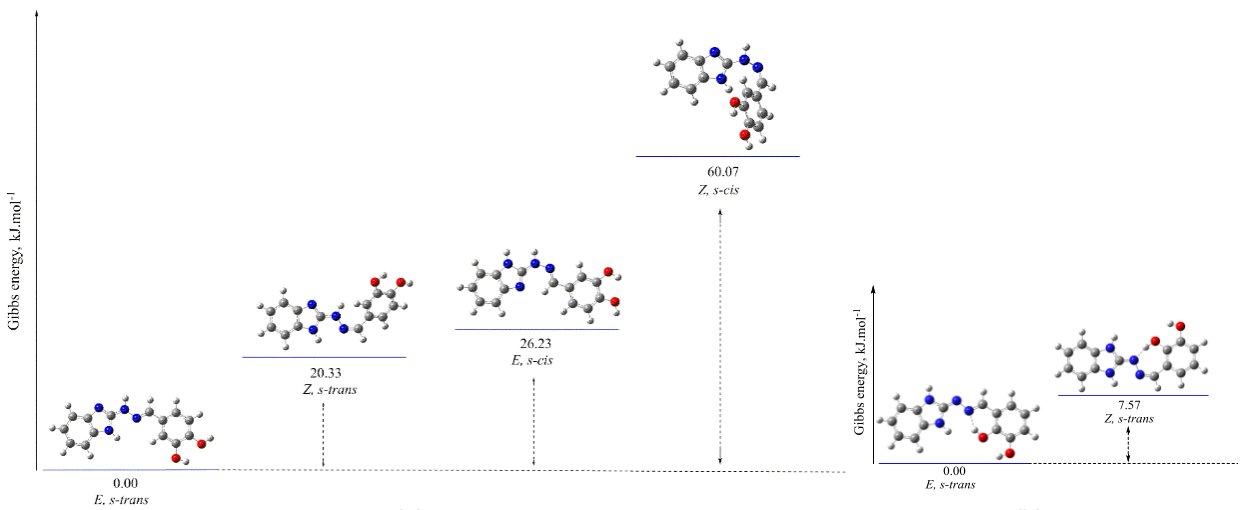

(a) *(b)*

*Figure 1. Optimized molecular structure and relative Gibbs energies (in kJ.mol^{-1}) of the possible isomers of compounds **5.17** (b) and **5.19** (a) in amino tautomeric form, obtained at B3LYP/6-311++G(d,p) level of theory in gas phase*

The gas-phase energy differences between the different isomers of the compounds **5.19; 5.21-5.24** and **5.27** with preferred amino forms are within the following ranges: *E, s-trans* → *E, s-cis* (ΔG 16.90-47.29 kJ/mol^{-1}) → *Z, s-trans* (ΔG 16.91-34.60 kJ/mol^{-1})

The gas-phase energy differences between the different isomers of the compounds **5.16-5.18; 5.20** and **5.25-5.26** with preferred imino forms vary as follows: *E, s-trans* → *E, s-cis* (ΔG 0.88-35.34 kJ/mol^{-1}) → *Z, s-trans* (ΔG 4.17-28.34 kJ/mol^{-1})

The theoretically estimated geometry of the amino *E, s-trans* forms is in a significant correlation with earlier reported X-ray experimental data. The calculated bond lengths of

compound **5.19** are close to the values of the benzimidazolyl-2-hydrazone of pyridine-2-carbaldehyde examined by Pervova et al. (Figure 2). The *trans* configuration of the double C=N bond of the target hydrazones is compatible with the reported structures of hydrazones containing benzothiazole as well as benzimidazole fragment.

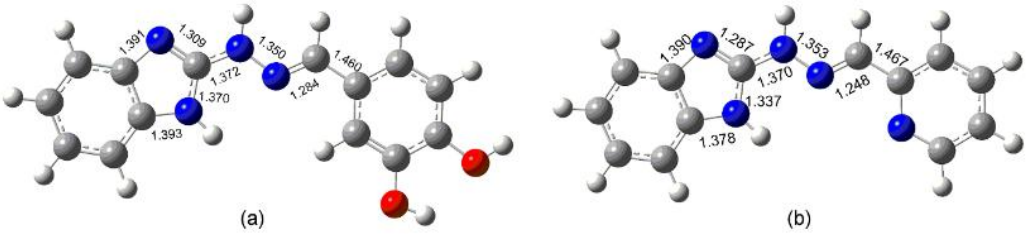

*Figure 2. General view of the molecule of compound **5.19** (a) and benzimidazolyl-2-hydrazone of pyridine-2-carbaldehyde (b) with selected bond lengths*

2.2. Molecular structure of 1H-benzimidazol-2-yl hydrazones containing a methyl group at 5(6)-position in the benzimidazole moiety

Similarly, in series C the imino form prevails in the hydrazones containing hydroxyl groups in *ortho*-position in the phenyl fragment (**5.28-5.30**; **5.32** и **5.37-5.38**). The amino form is the preferred one in the rest of the compounds (**5.31**; **5.33-5.36** и **5.39-5.40**). The energy difference varies in the range 1.97-11.19 kJ.mol^{-1}.

The obtained results are shown in Figure 3 with hydrazones **5.29** и **5.31.**

Based on the data for compound **5.31,** containing two hydroxyl groups at positions 3 and 4 in the phenyl ring, the amino:imino ratio is: 82.42:17.58 (gas phase); 91:9 (water); 82.16:17.84 (benzene). The results obtained with M06-2X functional are in agreement with those from the B3LYP calculations: 71.51:28.49 (gas phase); 96.22:3.78 (water); 92.22:7.78 (benzene) respectively.

For compound **5.29** the amino:imino ratio is 97.26:2.74 (gas phase); 90.28:9.72 (water); 99.23:0.77 (benzene) according to the B3LYP calculations and amino:imino ratio 96.64:3.36 (gas phase); 86.44:13.56 (water); 87.65:12.35 (benzene) according to the M06-2X functional.

The calculated Gibbs energies for the possible conformers of the methyl-substituted hydrazones of series B confirmed the above-mentioned conclusions, that the most favorable molecular structure is planar, the *E* configuration of the double bond and the *s-trans* conformation of the single N-N bond were observed (Figure 3).

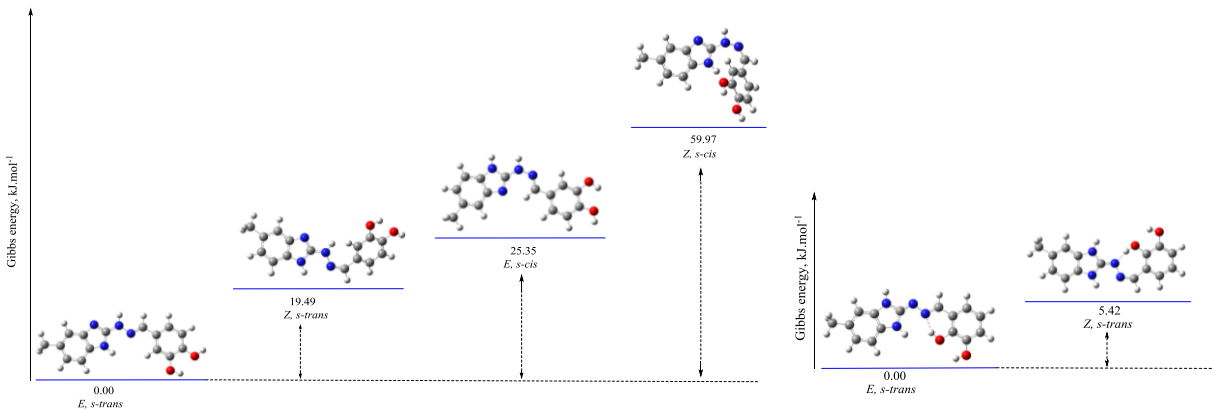

(a) *(b)*

*Figure 3. Optimized molecular structure and relative Gibbs energies (in kJ.mol^{-1}) of the possible isomers of compounds **5.31** (a) and **5.29** (b) in amino tautomeric form, obtained at B3LYP/6-311++G(d,p) level of theory in gas phase*

The gas-phase energy differences between the different isomers of the compounds **5.31**; **5.33-5.36** and **5.39-5.40** with preferred amino forms are within the following ranges: *E, s-trans* → *E, s-cis* (ΔG 8.46-47.26 kJ.mol^{-1}) → *Z, s-trans* (ΔG 9.84-37.08 kJ.mol^{-1}).

The gas-phase energy differences between the different isomers of the compounds **5.28-5.30**; **5.32** and **5.37-5.38** with preferred imino forms vary as follows: *E, s-trans* → *E, s-cis* (ΔG 0.98-37.13 kJ.mol^{-1}) → *Z, s-trans* (ΔG 0.52-12.25 kJ.mol^{-1}).

The calculated Gibbs energies indicated that for compounds **5.29** and **5.32-5.37** the 6-th position of the methyl group is preferred, while for hydrazones **5.28**; **5.30-5.31** and **5.38-5.40**, the 5-th position of the methyl group is more favourable. The energy difference varies between 0.20-3.87 kJ.mol^{-1}.

In addition, Figure 4 presents the calculated bond lengths for compound **5.31** and the values are very close to the data for hydrazone **5.19** from series B. Also, the obtained results are in excellent agreement with those published by Pervova et al.

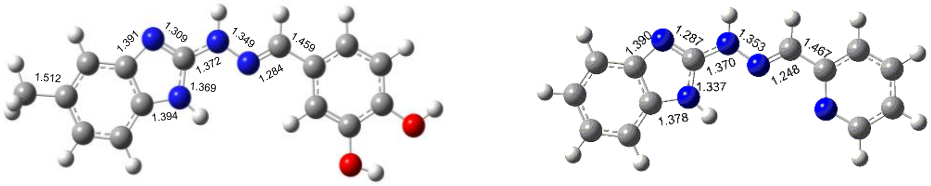

(a) (b)

*Figure 4. General view of the molecule of compound **5.31** (a) and benzimidazolyl-2-hydrazone of pyridine-2-carbaldehyde (b) with selected bond lengths*

*2.3. Molecular structure of the metal complexes **6.1-6.4***

The study of the molecular geometry and electronic structure of the synthesized metal complexes was enriched by DFT calculations. The optimization was carried out by applying B3LYP functional and LANL2DZ or 6-311++G(d,p) basis set. Two coordination modes were taken into account for each complex and were optimized. The first one is bidentate coordination with one ligand and the second - tridentate coordination with two ligands.

In accordance with the spectral data and elemental analysis, the theoretical calculations indicated that the most stable structures of the complexes correspond to coordination of one molecule benzimidazolyl hydrazone with one copper or iron atom (Figure 5). The molecule is planar and the coordination is observed between the copper (iron) atom with the nitrogen atom from the 3-position of the benzimidazole fragment, the nitrogen atom of the azomethine bond and the hydroxyl group in *ortho*-position of the phenyl moiety. In the structure of the complex there is also one chlorine atom connected to the metal atom.

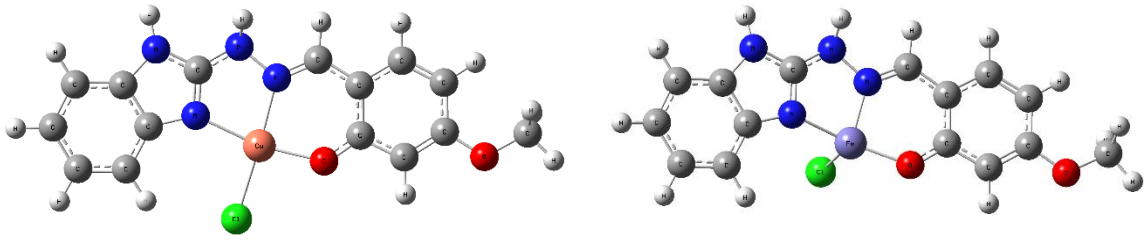

(a) (b)

*Figure 5. Optimized moleculat structure of the metal complexes **6.3** with copper atom (a) and complex **6.4** with iron atom (b), obtained at B3LYP/6-311++G(d,p) level of theory in gas phase*

3. Study of the pharmacological activities and potential mechanism of action

3.1. In vitro study of the antitrichinella and antineoplastic activity of 1H-benzimidazolyl hydrazones from series A

Having in mind that the anthelmintic effect might be related to the manifestation of antiproliferative activity mediated through modulation of tubulin polymerization, both the antiparasitic and antineoplastic activity of the newly 1*H*-benzimidazolyl hydrazones were studied *in vitro*.

The newly synthesized compounds from series A were screened for their *in vitro* anthelmintic activity against isolated *T. spiralis* muscle larvae and compared with the board-spectrum antinematodal agents albendazole and ivermectin which were used as reference drugs. The *in vitro* effect of the compounds on viability rates of *T. spiralis* muscle larvae after 24 h of exposure is presented in Figure 6. The tested benzimidazoles showed a remarkable larvicidal effect on *Trichinella* muscle larvae superior to that of albendazole and ivermectin. The experimental results allowed the identification of compounds **5.9.** and **5.10.** as the most potent antinematodal agents. They killed the total larvae (100 % effectiveness) after 24 hours in the concentrations of 100 μg/mL corresponding to 0.376 μM for **5.10.** and 0.396 μM for **5.9,** respectively. Derivatives **5.14.** and **5.5.** demonstrated 98.10 % and 91.23 % activities, accordingly, at the dose of 100 μg/ml for the same incubation period (24 h)(Figure 6).

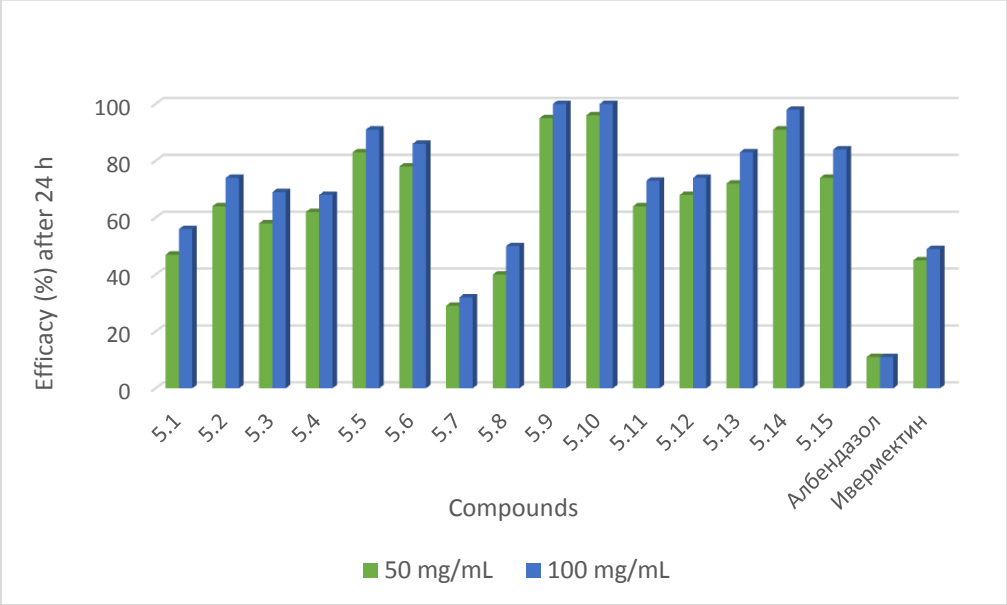

Figure 6. In vitro effect of compounds from series A on viability rates of T. spiralis muscle larvae after 24 h of exposure

The best results were obtained by the presence of a methyl function at 5(6)-position of the benzimidazole ring, as suggested by the molecular docking studies (see Section 3.5). Compound **5.10.** was distinguished for 82.70 % efficacy at a concentration of 12.5 μg/mL (0.047 μM), while derivative **5.9.**which does not contain a methyl group at 5(6)-position of the benzimidazole skeleton exhibited 79.23 % larvicidal effect at concentration 12.5 μg/mL,

relevant to 50 μM after 24 h. This trend was observed with less active analogues **5.14.** and **5.13.** as well as with **.5.** и **5.2**. Particularly, CH_3 group in 5(6)-position of benzimidazole heterocycle and OH substitution performed at *meta* position of phenyl moiety proved to be most productive, in fact, the introduction of OH substituent followed by OCH_3 group or F atom in C-3 of the phenyl portion of the molecule provided more potent analogs in comparison with the corresponding 4- or 2- substituted compounds. Comparing the hydrazones, the rank order of anthelmintic activity, according to the position and the nature of the substituent in the aryl fragment, is as follows: 3-OH > 3-OCH_3, 4-OH > 3-F > 4-OH > 4-F > 2-F. The larvacidal effects of tested compounds were dose- and time- dependent. The viability rates of *T. spiralis* larvae decreased with more prolonged exposure at all tested concentrations.

The benzimidazolyl-2-hydrazones of 1,3-benzodioxole-5-carboxaldehyde (compounds **5.7.** and **5.8.**) showed less pronounced effects against the parasites (less than 50%), comparable to that of the clinically approved anthelmintic ivermectin, after 24 h of exposure in the studied concentrations. In the control parasite samples (with physiological solution) *T. spiralis* larvae had spiral form *i.e.* are vital.

A study for *in vitro* cytotoxicity of some of the newly synthesized benzimidazole derivatives from series A has been further carried out in order to determine cell survival on a breast cancer human cell line MCF-7 (ER-positive breast adenocarcinoma) after treatment with compounds using the standard MTT-dye reduction assay and measurement of the absorption intensity of staining. In addition, the cytotoxicity of the compounds was tested towards normal cell line *3T3*. Cytotoxicity towards *MCF-7* corresponding to cell survival after incubation with the studied hydrazones was presented as a percentage to the cell viability of the positive control – non-treated cells.

Indeed, the studied benzimidazole derivatives bearing hydrazone moiety showed only low to moderate cytotoxic effect with a dose-dependent response and IC_{50} values in the range 16.54 – 95.54 μg/mL (Table 1).

Table 1. Antiproliferative activity towards MCF-7 and 3T3 cells of the newly synthesized hydrazones and the reference drug Nocodazole after 24 h continuous incubation (MTT-dye reduction assay).

Compounds	**Substituents**	**IC_{50} (μg/mL)**	
		MCF-7	***3T3***
5.6.	R_1=5(6)-CH_3; R_2= 4-F	34.60	24.7
5.9.	R_1=H; R_2= 3-OH	23.52	21.4
5.10.	R_1=5(6)-CH_3; R_2= 3-OH	16.54	19.4
5.12.	R_1=H; R_2= 3-OCH_3	91.42	-
5.13.	R_1=H; R_2= 3-OCH_3-4-OH	95.54	-
5.14.	R_1=5(6)-CH_3; R_2= 3-OCH_3-4-OH	17.40	16.7
5.15.	R_1=H; R_2= 3,5-diOCH_3-4-OH	21.54	-
Nocodazole		1.54	-

Hydrazones **5.10.**, **5.14.** and **5.15.** inhibited the growth of the cell line with low (< 25 μM) micromolar IC_{50} values. The substituted with hydroxyl group at 3-th position in benzene ring and with methyl group in 5(6)-th position in benzimidazole core compound **5.10.** demonstrated the most pronounced toxic effect to MCF-7 cells, IC_{50} = 16.54 μM, followed by the 4-hydroxy-3-methoxybenzylidene analog **5.14.** (IC_{50} – 17.50 μM). It can be assumed, that the increase of the cytotoxicity of benzimidazole analogues **5.10.** and **5.14.** versus **5.9.** and **5.13.** is related to the introduction of a methyl group at 5(6)-position of benzimidazole ring.

The introduction of the 4-hydroxy-3,5-dimethoxyphenyl moiety (compound **5.15.**) caused an increase in activity as compared with 4-hydroxy-3-methoxyphenyl derivative **5.13.** On the other hand, some above-mentioned compounds such as Colchicine and Combretastatin A4 shared a common 3,4,5-trimethoxyphenyl fragment in their chemical structures, implying this moiety might be crucial for their anti-tubulin polymerization activities and in this case the structure that is closest to it is 4-hydroxy-3,5-dimethoxyphenyl moiety (hydrazone **5.15.**). The established IC_{50} values show that the cytotoxicity of the tested compounds is much lower than those of the known microtubule targeting benzimidazole agent Nocodazole towards non-aggressive breast cancer cell-line, *MCF-7* (IC50 = 5.12 ± 0.07 μM, corresponding to 1.54 μg/mL). The cytotoxicity of studied benzimidazole derivatives towards mouse embryo fibroblasts *3T3* were in the same range as for *MCF-7* (Table 1), therefore not showing a selectivity among the tested cell lines.

Based on the gained results of the structure-activity relationship of the compounds from series A, it was concluded that expanding the range of 1*H*-benzimidazol-2-yl hydrazones by incorporating methoxy- and hydroxy-substituted phenyl moieties into their structure is a promising strategy for obtaining of new representatives with improved anthelmintic and antineoplastic activity.

3.2. In vitro study of the antitrichinella and antineoplastic activity of 1H-benzimidazolyl hydrazones from series B

The larvicidal effects of the newly synthesized compounds from series B on encapsulated *T. spiralis* ML were studied *in vitro*. The results, shown in Figure 7, indicated that all benzimidazoles in the tested concentrations were more active than the clinically used anthelmintic drugs Albendazole and Ivermectin.

The evaluation of the antihelmintic properties of the benzimidazole derivatives denoted that the hydrazones bearing only hydroxyl groups in the phenyl ring (compounds **5.16-5.20**) showed remarkable activity. Hydrazone **5.16** with a single hydroxyl group in 2-position of the phenyl ring exhibited 90 % larvicidal effect at concentration 100 $\mu g.ml^{-1}$ after 24 h. The introduction of a second hydroxyl group at 4-position of hydrazone **5.18** to give compound **5.16** produced 5 % enhancement in activity.

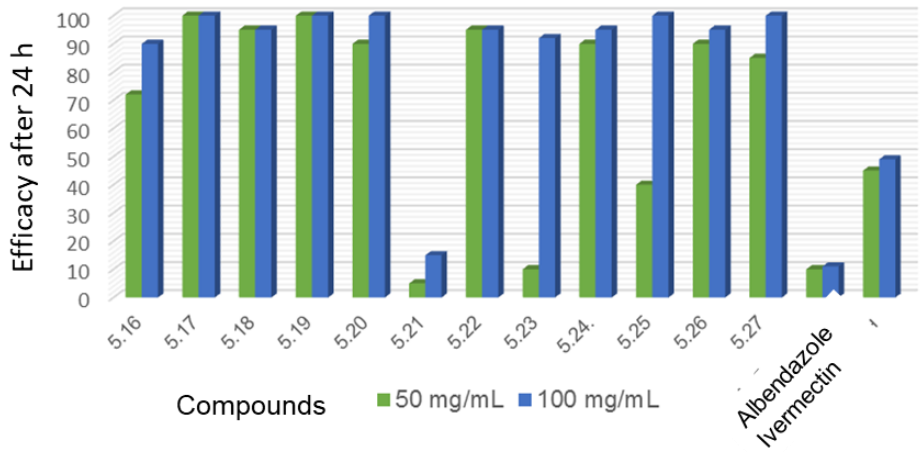

Figure 7. In vitro activity of compounds from series B against T. spiralis ML after 24 h of exposure

The shift of OH group from 4- to 3-position to give hydrazone **5.17** led to further increase in activity (100% efficacy at a concentration of 50 $\mu g.ml^{-1}$). In accordance with these

and our earlier results[18], it can be assumed that the presence of a OH group in the 3-position of the phenyl moiety of the molecule accounts for a larger share of the anti-*Trichinella spiralis* activity. The benzimidazolyl-2-hydrazone of 2,3-dihydroxybenzaldehyde (compound **5.17**) and of 3,4-dihydroxybenzaldehyde (compound **5.19**), respectively, killed the total parasitic larvae (100 % effectiveness after 24-hour incubation period at 37°C) in concentrations of 50 $\mu g.ml^{-1}$. A comparison of the biological effects revealed that the presence of two or three hydroxyl groups in phenyl moiety led to benzimidazole derivatives **5.17**; **5.18**; **5.19** and **5.20** endowed with a much better anthelmintic activity against *T. spiralis* as compared with that of the naturally occurring the stilbenoid polyphenol – resveratrol, which in study *in vitro* has showed a lethal effect on muscle *Trichinella* larvae only upon exposure to very higher concentrations (440 and 880 μM) for 72 h. On the other hand, there are numerous reports of natural phenolic compounds (including flavonoids) with anthelmintic effects against parasitic nematodes other than *T. Spiralis* and their anthelmintic activity increases with the number of hydroxyl groups.

However, the presence of a hydroxyl group at 3-position in combination with a 4-methoxyl moiety (compound **5.27**) led to slight reduction in activity (85 % larvicidal effect after 24 h in concentration of 50 $\mu g.ml^{-1}$) as compared to hydrazone **5.19**. Methoxy-analogues (**5.21** and **5.23**) showed less pronounced activities against the parasites, comparable to that of the anthelmintic Albendazole, after 24 h of exposure in 50 $\mu g.ml^{-1}$ concentration. The larvicidal effects of the tested compounds (excluding **5.21**; **5.23**; **5.25** and **5.27**) were dose-independent *i.e.* the viability of *T. spiralis* larvae was almost unchanged with 2-fold increase in the dose (100 $\mu g.ml^{-1}$).

Based on the *in vitro* activity of the target hydrazones on *T. spiralis* ML as well as hydrazones **5.1-5.15** from series A, it was outlined that the combination of benzimidazole and hydrazone pharmacophores in addition with hydroxyl and/or methoxyl groups on the arylidene moiety favorably modulates anti-*Trichinella spiralis* activity. Indeed, the studied benzimidazole hydrazones showed remarkable larvicidal effect superior to the compounds from series A as well as benzimidazole-containing derivatives earlier synthesized by some authors.

A standard colorimetric MTT assay was used to evaluate the anticancer activity of the newly synthesized 1*H*-benzimidazol-2-yl hydrazone derivatives from series B against human malignant cell lines of different histological origin, namely MCF-7 (ER-positive breast adenocarcinoma) and AR-230 (BCR-ABL positive chronic myeloid leukemia), using podophyllotoxin as a reference drug. For each compound, the half-inhibitory concentrations (IC_{50}) were estimated based on the derived "dose-response" relationships following 72h exposure time. In addition, their cytotoxicity was measured against normal murine fibroblast cells CCL-1 and respective cancer selectivity indices (CSI) were calculated (Table 2).

Table 2. In vitro cytotoxicity of 1H-benzimidazole-2-yl hydrazones from series B against cell lines of different origin.

Comp.	Substituents	IC_{50} (μM)			CSI	
		MCF-7	AR-230	3T3/CCL-1	CSI_{MCF-7}	CSI_{AR230}
5.16.	R_1=H; R_2= 2-OH	18.7 ± 1.1	21.2 ± 2.3	204±5.1	≈ 11	≈ 9.6
5.17.	R_1=H; R_2= 2,3-diOH	64.5 ± 6.2	**3.3 ± 0.3**	61.1±1.8	≈ 1	≈ 18.4
5.19.	R_1=H; R_2= 3,4-diOH	-	61.8 ± 5.7	112.8 ± 9.1	≈	≈ 1.8
5.21.	R_1=H; R_2= 4-OCH_3	11.2 ± 1.3	19.4 ± 2.2	355±5.3	≈ 31.6	≈ 18.2
5.22.	R_1=H; R_2= 2,6-diOCH_3	7.9 ± 2.1	11.5 ± 1.0	261±4.7	≈ 33	≈ 22.6
5.23.	R_1=H; R_2= 3,5-diOCH_3	4.6 ± 0.7	5.9 ± 0.9	335±7.0	≈ 72.8	≈ 56.7
5.24.	R_1=H; R_2= 3,4,5-triOCH_3	**1.2 ± 0.2**	**1.7 ± 0.3**	71±2.4	≈ 59.1	≈ 41.7
5.25.	R_1=H; R_2= 2-OH-3-OCH_3	6.4 ±1.2	1.1 ± 0.2	> 400	≈ 62.5	≈ 363.6

5.26.	R_1=H; R_2= 2-OH-4-OCH_3	**1.5 ± 0.3**	**0.9 ± 0.1**	101.8 ± 7.3	≈ 67.8	≈ 113
5.27.	R_1=H; R_2= 3-OH-4-OCH_3	27.6 ± 3.5	16.8 ± 3.4	134.7±1.3	≈ 4.8	≈ 8
	Podophyllotoxin	0.3 ± 0.06	0.47 ± 0.09	2.7	≈ 9	≈ 5.7

As indicated by the presented experimental data, the newly synthesized benzimidazole compounds demonstrate a marked antineoplastic activity in low micromolar concentrations in both screened *in vitro* tumor models. The leading structures of the series include the trisubstituted benzimidazole derivative 3,4,5-trimethoxyphenylbenzimidazol-2-yl-hydrazone (**5.24**) (IC_{50} = 1.2 μM спрямо *MCF-7* и IC_{50} = 1.7 μM спрямо *AR-230*); as well as the disubstituted positional isomers **5.25** and **5.26** 2-hydroxy-3-methoxyphenylbenzimidazol-2-yl-hydrazone and 2-hydroxy-3-methoxyphenylbenzimidazol-2-yl-hydrazone. Their half-inhibitory concentrations (IC_{50}) in both tumor cell lines are similar to those of the reference drug, but in contrast, the benzimidazole derivatives are distinguished by high selectivity with regard to malignantly transformed adenocarcinoma and leukemic cells compared to the normal CCL-1 cell culture. The determined CSIs for the three compounds were strictly > 50 in both tumor cell lines, whereby the highest tumor selectivity exhibited the disubstituted ortho-position isomer **5.25** against AR-230 myeloid cells (CSI ≈ 363).

The cytotoxicity data for two of the most potent compounds in the series **5.25** и **5.26** are consistent with the results from the tubulin assay presented in section 3.5. Thereby, both heterosubstituted analogues had a great impact on the rates of tubulin polymerization increasing the lag time of the process to more than 20 minutes. Interestingly, the most efficient modulators of tubulin kinetics (lag time of 1400s), the **5.17** and **5.19** benzimidazoles lacking a OCH3 group, displayed the poorest cytotoxicity and cancer selectivity in the series. Considering this, alternative additional mechanistic properties are likely to be involved in the antitumor effects of the experimental compounds.

A certain "structure-activity" relationship was also observed between the analogues in the series, according to which their activity decreases in the order: **5.25**, **5.26** (ortho/meta heterosubstituted derivatives with both -OH and -OCH_3 groups in the benzylidene ring) > **5.22**, **5.23** (disubstituted analogues with two -OCH_3 methoxy groups in meta position) > **5.16**, **5.21** (monosubstituted benzimidazoles with a hydroxyl- or methoxy-group in the benzylidene core) > **5.17**, **5.19** (dihydroxy-substituted benzylidene ring). Favorably, the cancer selectivity of the compounds follows a reciprocal pattern. Based on this, it can be concluded that the two substituents -OH and -OCH_3 are key pharmacophore elements and their mutual presence in the structure of the experimental compounds synergistically improves their antitumor activity and cancer selectivity.

The cell viability of MCF-7 and AR-230 cell lines following 72h exposure to compounds **5.25** and **5.26** are illustrated in Figure 8.

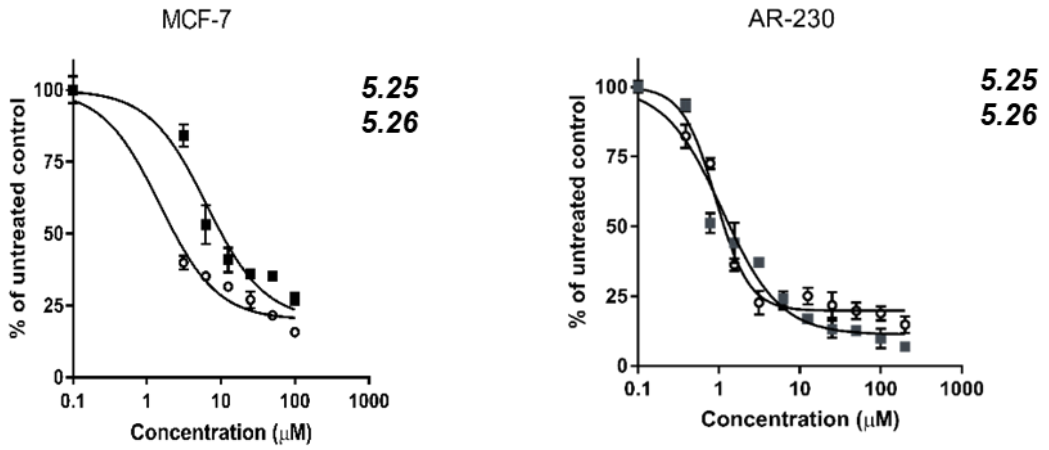

(a) (b)

Фигура 8. Cell viability of MCF-7 (a) and AR-230 (b) cell lines following 72h exposure to the lead compounds 1H-benzimidazole-2-yl hydrazones ***5.25 and 5.26***

3.3. In vitro study of the antitrichinella and antineoplastic activity of 1H-benzimidazolyl hydrazones from series C

The results from the *in vitro* assessment of the larvicidal effect of the synthesized compounds from series C on encapsulated *T. spiralis* ML after 24- and 48-hours incubation and concentrations 100 и 50 μg.ml^{-1}, are presented in Figure 9. All derivatives in the tested concentrations were more active than the clinically used anthelmintic drugs Albendazole and Ivermectin.

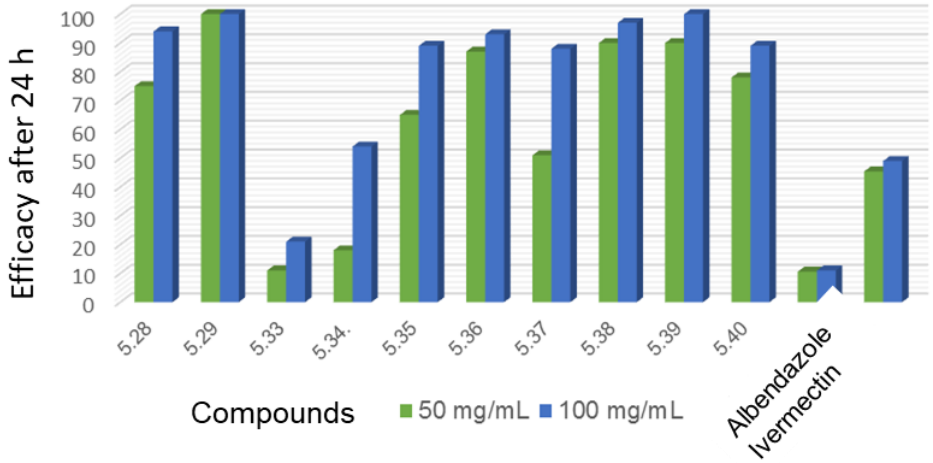

Figure 9. In vitro activity of compounds from series C against T. spiralis ML after 24 h of exposure

Hydrazones (**5.28** and **5.29**) that contain in the phenyl ring hydroxyl groups exhibited activity from 75% to 100% against *T. Spiralis larvae* after 24 and 48 hours of incubation period for both concentrations. Compound **5.29**, whose substituents in the phenyl fragment are hydroxyl groups at *ortho*- and *meta*-position, possessed the highest activity among the series B (100% efficiency at concentrations of 50 and 100 μg.ml^{-1}), after 24 hours and 48 hours of incubation. Derivatives with substituents hydroxyl- and methoxyl groups in the phenyl core also showed high efficacy such as hydrazone **5.39** with 100% activity after 48 h of incubation at both concentrations. According to the obtained results, the presence of a

hydroxyl group at the 3-position of the phenyl residue (hydrazones **5.29** and **5.39**) is a crutial for revelaling a stronger anthelmintic effect.

The hydrazones with methoxyl groups in the phenyl moiety **5.33-5.35** showed a less pronounced effect, especially at the lower tested concentration 50 μg.ml^{-1}. Compound **5.33** exhibited the lowest effect, only 11%, after 24 hours of incubation at a concentration of 50 μg.ml^{-1}. The hydrazone, which contains three methoxy groups in the phenyl ring - **5.36** exhibited the most potent effect (93% at a concentration of 100 μg.ml^{-1} after 24 hours of incubation) among the methoxyl analogues.

The presence of methyl groups as a substituent in the benzimidazole heterocycle does not influence significantly the anthelmintic activity. It could be concluded that the presence of two hydroxyl groups in the phenyl moiety or combination of hydroxyl- and methoxyl substituents is more important for the manifestation of higher activity. All tested hydrazones of series C showed stronger effect than Albendazole and Ivermectin.

The *in vitro* cytotoxicity of the 1*H*-benzimidazol-2-yl hydrazones from series C was studied towards the tumor cell lines *MCF-7 и AR-230* and against normal cell line *3T3* (Table 3).

Table 3. In vitro cytotoxicity of 1H-benzimidazole-2-yl hydrazones from series C against cell lines of different origin

Comp.	Substituents	IC_{50} (μM)		
		MCF-7	AR-230	3T3
5.28.	R_1=CH_3; R_2= 2-OH	**6.9 ± 0.3**	**2.2 ± 0.5**	80.6
5.29.	R_1=CH_3; R_2= 2,3-diOH	**3.4 ± 0.5**	**1.9 ± 0.4**	235
5.33.	R_1= CH_3; R_2= 4-OCH_3	31.4 ± 3.4	20.1 ± 4.2	257
5.34.	R_1= CH_3; R_2= 2,6-diOCH_3	15.7 ± 2.1	18.7 ± 3.7	84.3
5.35	R_1=CH_3; R_2= 3,5-diOCH_3	67.2 ± 3.8	116.9 ± 10.9	240
5.36.	R_1=CH_3; R_2= 3,4,5-triOCH_3	51.2 ± 4.7	**3.0 ± 0.6**	509
5.37.	R_1= CH_3; R_2= 2-OH-3-OCH_3	**6.4 ± 1.2**	**3.0 ± 0.1**	-
5.38.	R_1= CH_3; R_2= 2-OH-4-OCH_3	**1.5** ± **0.3**	**2.3 ± 0.6**	-
5.39	R_1= CH_3; R_2= 3-OH-4-OCH_3	103.0 ± 8.2	51.2 ± 6.8	-
5.40.	R_1= CH_3; R_2= 3,5-diOCH_3-4-OH	> 200	12.4 ± 2.3	-
Podophyllotoxin		0.3 ± 0.06	0.47 ± 0.09	

The IC_{50} values of the 1*H*-benzimidazol-2-yl hydrazones from series C towards the cell lines varied in the range: 1.5-116.9 μM. Compound **5.38.** showed the lowest IC_{50} value towards the MCF-7 cell line: 1.5 μM. When comparing analogues **5.16.** from series B and **5.28.** from series C (both with a hydroxyl group at the *ortho*-position in the phenyl moiety, but distinguished by the methyl group in the benzimidazole heterocycle), whose IC_{50} values were 18.7 μM (MCF-7) and 21.2 μM (AR-230), respectively for **5.16**., and 6.9 μM (MCF-7) and 2.2 μM (AR-230) for **5.28**., it could be concluded that the introduction of a methyl group as a substituent in the benzimidazole core is favorable for obtaining higher cytotoxicity. The same trend was observed for compounds **5.29.** (3.4 μM (MCF-7) and 1.9 μM (AR-230)) and **5.17.** (64.5 μM (MCF-7) and 3.3 μM (AR-230)). The methoxy derivatives from series C **5.33.-5.36**. exhibited lower cytotoxicity towards the two cell lines compared to the analogues from series B, except the hydrazone **5.36.** which showed IC_{50} = 3.0 μM towards AR-230.

For the hydrazones from series C containing hydroxyl- and methoxyl groups at the 3- and 4-position in the phenyl residue (**5.27.** with IC_{50} = 27.6 μM against MCF-7 and 16.8 μM against AR-230; **5.39.** with IC_{50} = 103.0 μM vs. MCF-7 and 51.2 μM vs. AR-230), the

introduction of a methyl group in the benzimidazole fragment leads to a decrease in the cytotoxicity compared to their analogs from series B. On the other hand, compound **5.38.**, which also contains hydroxyl- and methoxyl-groups in the phenyl core, but in *ortho*- and *para*-position, exhibited the highest cytotoxicity amond the hydrazones from series C towards the two cell lines MCF-7 (1.5 μM) and AR- 230 (2.3 μM). In addition, the hydrazone of 2-hydroxy-3-methoxy-benzaldehyde (**5.37.**) also possessed a pronounced cytotoxic effect towards the cell line AR-230 (3.0 μM).

3.4. In vitro study of the antineoplastic activity of metal complexes of the 1H-benzimidazol-2-yl hydrazones

The *in vitro* cytotoxicity of the obtained metal complexes **6.1.** и **6.3.** was elucidated towards the tumor cell lines *MCF-7* and *AR-230* as well as towards the normal cell line *CCL-1* (Table 4).

Table 4. In vitro cytotoxicity of metal complexes of the 1H-benzimidazole-2-yl hydrazones towards cell lines of different origin

Comp.	IC_{50} (μM)		
	MCF-7	AR-230	CCL-1
6.1.	2.3 ± 0.2	8.6 ± 0.4	4.4 ± 1.0
6.3.	1.8 ± 1.0	n.d. (>400)	10.5 ± 0.3
Podophyllotoxin	0.3 ± 0.06	0.47 ± 0.09	

The studied metal complexes **6.1.** and **6.3.** exhibited cytotoxic activity in low micromolar concentration range towards the cell lines MCF-7 and AR-230. Significant differences in the cytotoxicity were observed between ligands **5.16.** and **5.26.** and the copper complexes **6.1.** and **6.3.** towards the normal CCL-1 cell line. The ligands possessed negligible antiproliferative activity against the line CCL-1, indicating selectivity with calculated selectivity indices >100. On the other hand, their metal complexes (**6.1.** and **6.3.**) could not exert high selectivity due to kinetic stability factors. In addition, an increase in the activity of complex **6.1** was observed against line MCF-7 (IC50=2.3 ± 0.2 μM) compared to the ligand **5.16.**, from which it was derived (IC50=18.7 ± 1.1 μM).

3.5. In vitro effect on tubulin polymerization and molecular docking study on the tubulin-ligands interactions

The ability of the compounds to modulate the tubulin polymerization was evaluated *in vitro* on purified porcine tubulin by spectrophotometric monitoring at 350 nm and compared to those of nocodazole and paclitaxel as reference compounds. Nocodazole which inhibits the assembly of tubulin was used as a positive control, and paclitaxel which is a stabilizing agent of tubulin polymerization was used as a negative control. Tubulin polymerization was determined with 10 μM of the reference drugs and compounds for 90 min.

The kinetic curves for the tubulin polymerization in the presence of two benzimidazole derivatives from series A (**5.9** and **5.14**) as well as control experiments with paclitaxel and nocodazole, two known tubulin polymerization modulators, are depicted in Figure 10.

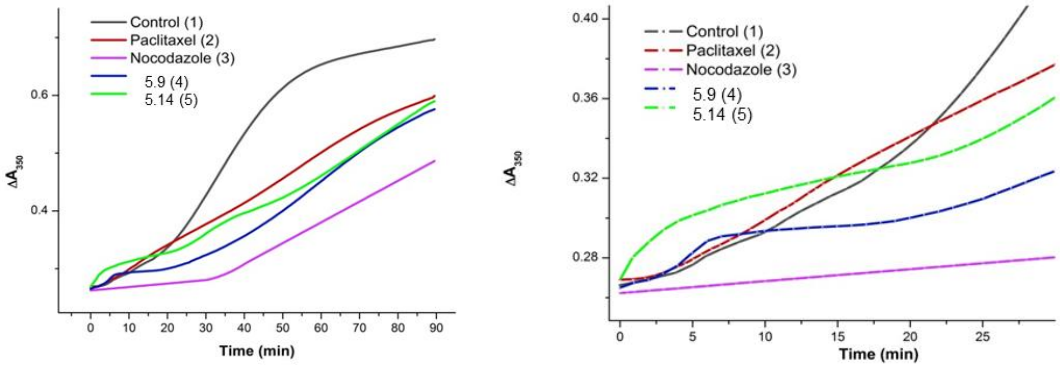

(a) (b)

*Figure 10. Tubulin (final 54 μM) in presence of PB-GTP buffer (1), 10μM paclitaxel (2), 10μM nocodazole (3), 10 μM **5.9** (4), and 10μM **5.14** (5): (a) represents the whole kinetic curve, (b) represents the enlarged first phase of polymerization.*

For the spontaneous polymerization of tubulin (curve 1) are clearly visible the three phases of polymerization: nucleation, growth, and steady state equilibrium. Expectedly, for palixatel lag time is not visible due to fast start of the growth phase. A decrease in tubulin polymerization rate was observed in the presence of **5.9**, **5.14** and nocodazole. Interestingly, the two tested compounds prolong the lag period (nucleation time) in the tubulin polymerization.

The kinetic curves for the tubulin polymerization in the presence of benzimidazole derivatives from series B and C are depicted in Figure 11.

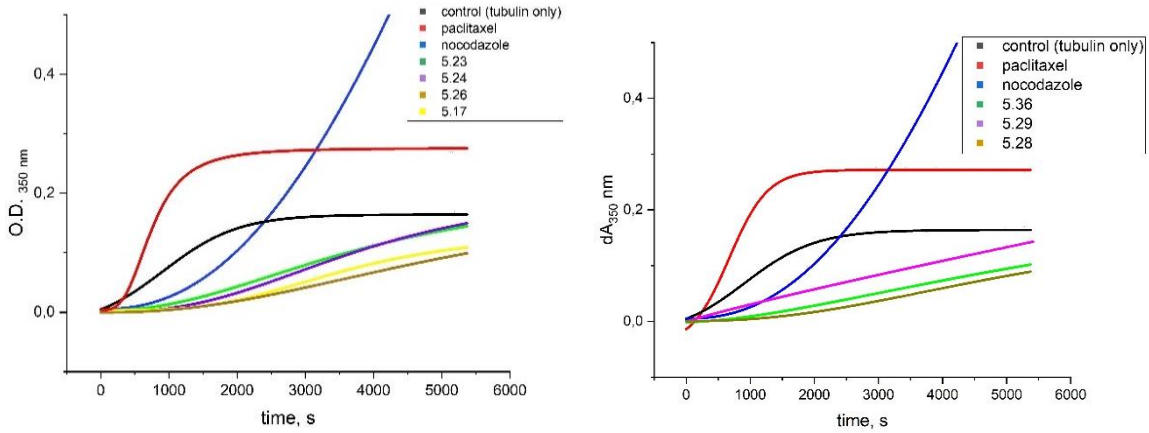

(a) (b)

*Figure 11. Tubulin (final 54 μM) in presence of PB-GTP buffer (1), 10μM paclitaxel (2), 10μM nocodazole (3), 10 μM of the tested hydrazones (a) **5.23; 5.24; 5.26** and **5.17** from series B and (b) **5.36; 5.29** and **5.28** from series C*

It was found that compounds **5.16**-**5.27** from series B modulate the polymerization of tubulin at different extend depending on their molecular structure. All of them, except for **5.27**, elongated the nucleation phase and all slowed down the tubulin polymerization in a higher extend than nocodazole.

Depending on the measured lag time (time of nucleation) and initial rates of the polymerization phase, the compounds within the series could be divided into three subgroups. The first of them encompasses the derivatives containing only hydroxyl substituents in the phenyl ring **5.16-5.20**: they elongated the nucleation phase up to 1000-1461 sec and slowed down the polymerization to 4.9-13.4 a.u.sec^{-1}.10^{-6}**.** In comparison, the spontaneous tubulin polymerization occurs at initial rate of 75.3 a.u.sec^{-1}.10^{-6} and the

modulating effect of nocodazole is related to lowering of the initial rate to 52 a.u.sec^{-1}.10^{-6}. The second subgroup among the studied compounds – those containing only methoxy substituents in the phenyl ring **5.21-5.24**, showed shorter lag times (807-1090 sec) and slightly higher initial rates of polymerization (10.7-23.1 a.u.sec^{-1}.10^{-6}). The third subgroup – including the derivatives containing both hydroxyl and methoxy substituents in the phenyl ring **5.25-5.27**, showed intermediate values of the two parameters: lag times of 1200-1295 s and initial rates of polymerization of 9.7-16.9 a.u.sec^{-1}.10^{-6}**.** In the case of **5.27** no lag phase was observed.

The kinetic curves for the tubulin polymerization in the presence of benzimidazole derivatives from series C and the reference drugs paclitaxel and nocodazole are presented in Figure 11b. The compounds of series C were found to exhibit a distinct modulation effect on polymerization of tubulin and among the obtained hydrazones there is no lag time (time of nucleation), but initial rates of the polymerization phase were significantly reduced over a long time interval, as seen in Figure 11b. This group includes two derivatives containing hydroxyl substituents in the phenyl ring - **5.28.** and **5.29.**, and two methoxy-analogs - **5.33.** and **5.34.** They could slow down the polymerization to 3-27 a.u.sec^{-1}.10^{-6}. The two methoxy-substituted compounds - **5.35.** and **5.35.**, exhibited a lag time of 600-845 sec and low initial rate of polymerization (12.9-23.6 a.u.sec^{-1}.10^{-6}).

To reveal the mode of ligand-tubulin interaction, docking studies were employed. According to the literature, the benzimidazole derivatives could bind to the tubulin at the colchicine binding site. The studies were carried out using the Schrödinger software package. The docking results clearly show that the addition of methyl group to benzimidazole core, as in the case of **5.10** from series A, better stabilizes the ligand by hydrophobic interactions with Thr314 and Ile347 (Figure 12A). The OH group makes a hydrogen bond with the backbone of Val238 which is significant for the ligand binding and observed activity. The introduction of OCH_3 substituent at position C-5, as in the case of **5.15**, cannot be accommodated due to the close position of Leu242, which leads to disruption of the aftermentioned H-bond and decreases activity. Indeed, the hydroxyl replacement with fluorine atom has the same effect. On the other hand, the substitutions at position C-3 would be well tolerated and provide hydrophobic contacts with Ile318 and Ile378 (Figure 12). The last is evident from the observed similar activity of ligands **5.10** and **5.14**. Calculated binding affinities of these compounds were in the range of about -6.5 kcal/mol which correspond to the observed IC_{50} values and larvacidal efficacy thus proposing a correlation between ligand-tubulin interactions and pharmacological activity.

A)

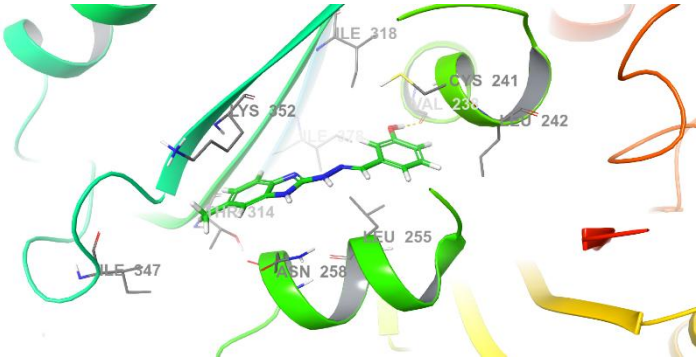

B)

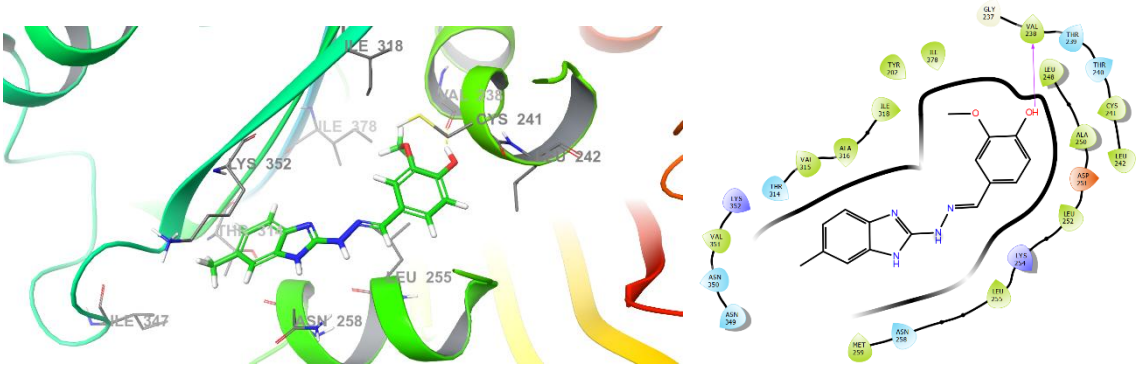

Figure 12. Retreived by the docking study binding modes of (A) ***5.10*** *in tubulin and (B)* ***5.14*** *2D representation of the observed* ***5.14****-tubulin interactions obtained our docking study.*

The possible binding modes of the 1*H*-benzimidazol-2-yl hydrazones from series B and C with tubulin were explored by molecular docking at the colchicine binding site of a complex of αβ-tubulin with colchicine and vinblastine, PDB ID: 1Z2B. Molecular docking study was performed by using MOE program package. The interactions of selected ligands – **5.17** and **5.24** with the tubulin dimer are illustrated in Figure 13. The positions of the ligands in the active pocket of colchicine are shown in the left part of the figure, where the docked structures are depicted by balls and sticks, and GTP is depicted by sticks. The interaction maps are shown in the right part of Figure 13.

Three of the illustrated compounds **5.17** and **5.24** from series B are accommodated in the active pocket with their benzimidazole ring oriented towards the hydrophobic amino acid residues Leu248, Ala250, Leu255, Met259, Val315, Ala316 and Ala318 of β-tubulin. The phenyl moieties of the compounds are oriented towards the polar amino acid residues of α-tubulin: Asn 101, Glu183, Asn249 and Tyr 224. The phenyl rings in hydrazones **5.17** and **5.24** are in close proximity of GTP and can interact with the polar amino acid residues Ser178 and Thr179 of α-tubulin T5 loop; Gln11 in T1 loop of α-tubulin and Lys254 within the H8 helix of β-tubulin, respectively. As it was previously reported for other tubulin inhibitors binding to the colchicine site such interactions play a role in the inhibition of the tubulin assembly by preventing the “curved-to-straight” conformational change. As Figure 13 shows, the binding of compounds **5.17** and **5.24** to tubulin is expected to be driven by Van der Waals interactions.

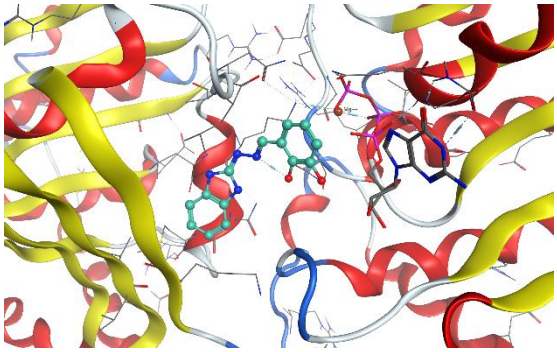

(a)

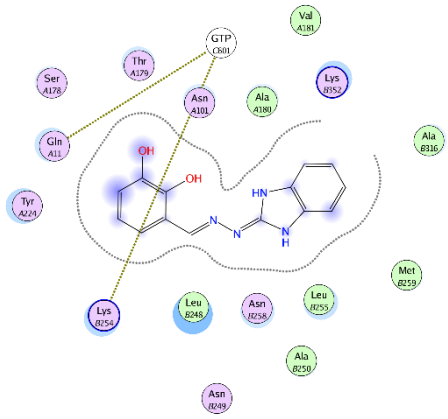

(b)

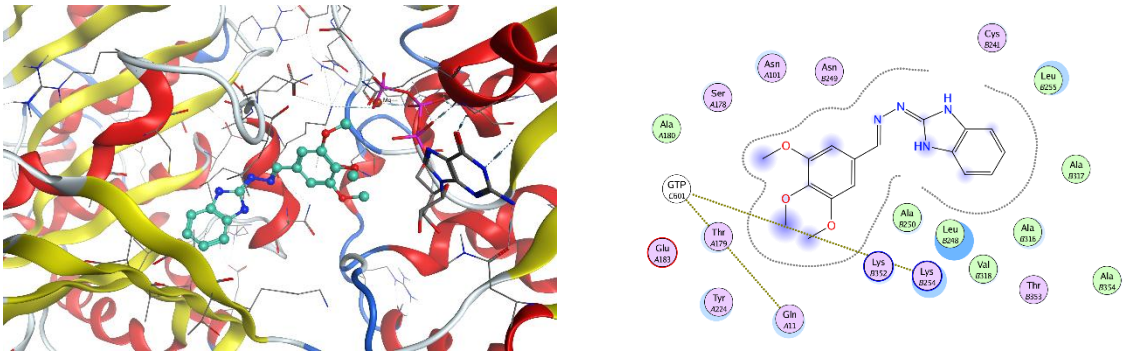

(c) (d)

*Figure 13. Three-dimensional (3D) representation of the interactions of ligands **5.17** (a) u **5.24*** (c) *at the colchicine binding site of the tubulin dimer (left part) and interaction maps (right part); the following colours have been used for representing the different components: the proximity contour – depicted by a black dotted line, polar amino acids – pink, lipophilic amino acids – green, basic amino acids – blue, acidic amino acids – red; hydrogen bond interactions – depicted by blue arrows, lipophilic interactions – green dotted lines. Docked structures are depicted by the balls and sticks, while GTP is depicted by sticks.*

The results from the molecular docking of hydrazone **5.38** from series C in the active site of colchicine are illustrated in Figure 14. The methyl group in the benzimidazole fragment is oriented towards the polar amino acid residues Gln11, Tyr224 and Asn101 of α-tubulin while the phenyl ring - towards the lipophilic residues Met259, Ala316, Val351 and Val315 of β-tubulin. There is a possibility of formation of hydrogen bond between the nitrogen atom at the 3-position in the benzimidazole core of **5.38** and the amino acid Ala250 of β-tubulin, which stabilizes the molecule in the pocket. In addition, a hydrogen bond is observed between the OH group in the *ortho*-position in the phenyl moiety and the amino acid Met259 of β-tubulin, which leads to additional stabilization in the active site of the colchicine.

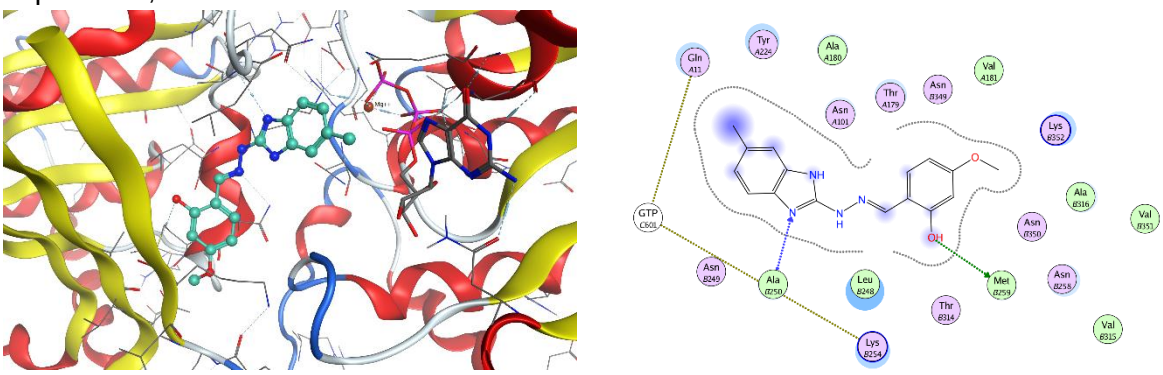

(a) (b)

*Figure 14. Three-dimensional (3D) representation of the interactions of ligands **5.38** at the colchicine binding site of the tubulin dimer (a) and interaction map (b)*

3.6. Experimental estimation of the radical scavenging and antioxidant activity

3.6.1. Study of the radical scavenging effects of the new 1H-benzimidazole-2-yl hydrazones against stable free radicals

The observed radical scavenging effects of the new 1*H*-benzimidazole-2-yl hydrazones against stable free radicals ABTS and DPPH are illustrated in Figure 15A and B. The performed experiments denoted that the absorbance values of the working solutions of both radicals decreased as the sample concentrations of the tested compounds increased. The curves for the relationship between concentration and radical scavenging activity,

obtained on the basis of these results, were with well-expressed linear dependences (R^2 < 0.95). They were used to estimate the C-50 values of the compounds and to compare their scavenging activity.

Two known antioxidants – quercetin and melatonin, were used as reference compounds in the experiments in order to judge better on the relative radical scavenging properties of the 1*H*-benzimidazole-2-yl hydrazones. Melatonin contains an indolyl heterocycle, structurally close to the benzimidazole one, while quercetin is a flavonoid compound including a catechol fragment which is also a structural unit relevant to the hydrozones studied in this dissertation.

The data obtained from the ABTS model system denoted C-50 values of the studied 1*H*-benzimidazole-2-yl hydrazones (**5.16.-5.27.** from series B) close or lower than that of the reference melatonin. The hydrazones bearing only methoxy groups in the phenyl ring (mono-, di- and tri-methoxy) had higher C-50 values compared to the references, suggesting necessity of higher amount of these compounds compared to melatonin and quercetin in order to achieve 50% RSA. Within this group of compounds, **5.23.** was the least active – with the highest observed C-50 value – 14.30 μmol.l^{-1}. **5.21., 5.22.** and **5.24**. had statically identical C-50 values. They were lower compared to **5.23.** suggesting better scavenging activity. **5.21.** had an equivalent C-50 value with the mono-hydroxyphenyl hydrazone **5.16.**

The presence of both methoxy and hydroxy groups in the tested 1*H*-benzimidazole-2-yl hydrazones induced significant decrease in the C-50 value compared to **5.21.** и **5.16.** The C-50 values of this subgroup comprising **5.25-5.27.** were lower than 8 μmol.l^{-1}. They demonstrated necessity of lower concentration of the active substance to induced 50% decrease of the RSA% compared to melatonin, but did not reach the C-50 concentration of quercethin.

The di- and trihydroxy substituted 1*H*-benzimidazole-2-yl hydrazones **5.17-5.20.** demonstrated the best RSA within the whole series. They had very similar and in some cases even identical C-50 values ranging from 4.15 to 5.20 μmol.l^{-1}. The observed effect was much higher compared to melatonin, but still did not reach the quercetin's effectiveness.

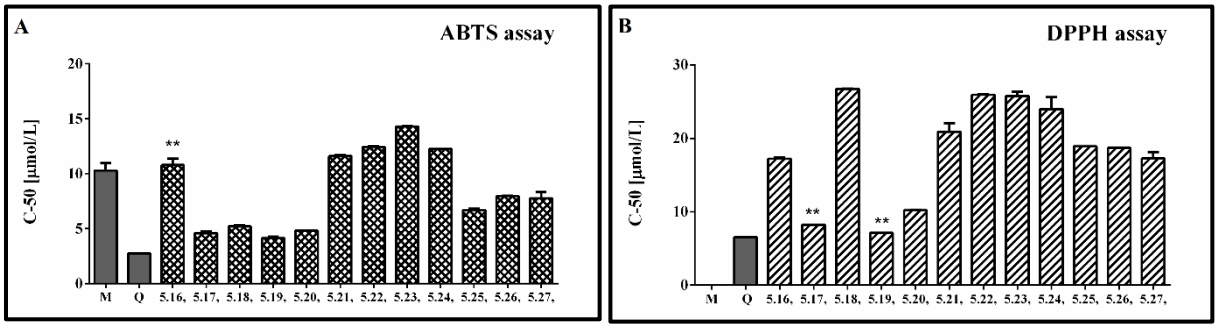

*Figure 15. Anti-radical properties of compounds **5.16-5.27.** from series B in spectrophotometric model systems containing the stable free radicals ABTS (A) u DPPH (B)*

In the DPPH model system, the reference melatonin did not exert capability to decrease the absorbance value of the radical solution. As observed in the ABTS system, among the group of the di- and trihydroxy substituted benzimidazoles were the most potent scavengers. The C-50 value of **5.20.** was slightly higher than quercetin (with a statistically significant difference). **5.17.** and **5.19.** denoted identical concentration as the mentioned reference. The hydrazone with the mono-hydroxyphenyl moiety **5.16.** and the hydrazones with mixed methoxy/hydroxy substitution *i.e.* **5.25-5.27** showed equivalent C-50 values. The compounds with di- and trimethoxyphenyl moiety, similarly to the ABTS system, exerted the highest C-50 values together with the dihydroxy substituted benzimidazoles **5.18**.

The radical scavenging effects of the new 1*H*-benzimidazole-2-yl hydrazones from series C against the stable free radicals ABTS and DPPH are illustrated in Figure 16A and B. Quercetin and melatonin were used as reference compounds. As the results for series B, the absorbance values of the working solutions of both radicals decreased as the sample concentrations of the tested compounds increased.

The results obtained from the ABTS model system denoted that the C-50 values of the studied 1*H*-benzimidazole-2-yl hydrazones are close or lower than that of the reference melatonin. On the other hand, the radical scavenging activity for the synthesized hydrazones from series C in the analogous system was significantly lower compared to the second reference antioxidant quercetin. Mono-, di- and tri-methoxy-substituted benzimidazoles **5.33.-5.36.** had higher C-50 values than the reference compounds, suggesting necessity for higher concentrations of these compounds to achieve 50% RSA% compared to melatonin and quercetin. Compound **5.33.** exhibited the lowest activity, although statistically it is comparable to that of compounds **5.28**., **5.35.** and **5.34.**

The introduction of hydroxyl- and methoxyl substituents in the phenyl ring (**5.37.-5.39**.) leads to an improvement of the activity compared to the methoxyl analogues (**5.33-5.36**.) and the radical-scavenging ability is similar or better than the effect of melatonin.

The hydrazone of 2,3-dihydroxy benzaldehyde (**5.29.**) demonsrated the most pronounced ability to eliminate the ABTS radical among the series, with a C-50 value of 5.52 μmol.l^{-1}.

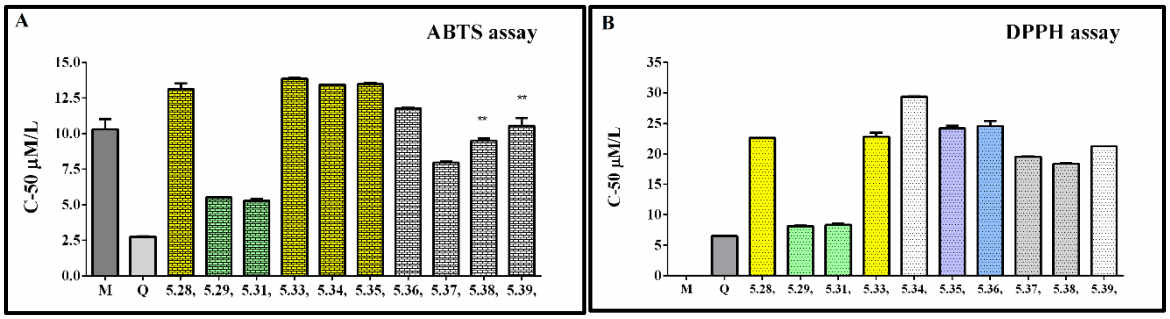

*Figure 16. Anti-radical properties of compounds **5.28-5.39.** from series C in spectrophotometric model systems containing the stable free radicals ABTS (A) u DPPH (B)*

In the DPPH model system, the reference melatonin did not exert capability to decrease the absorbance value of the radical solution. The presence of one or more methoxyl groups in the hydrazone (**5.33.-5.36**.) is associated with reduced radical scavenging activity. Hydrazones with methoxyl- and hydroxyl groups in the phenyl moiety (**5.37-5.39**.) leads to a modest but statistically significant decrease in the C-50 values compared to mono-, di-, and tri-methoxy-substituted benzimidazoles in the DPPH system.

Based on the observed decrease in absorbance of the ABTS and DPPH model systems and the possible interactions with the newly obtained compounds, was concluded that all of the compounds have the ability to eliminate the radicals.

3.6.2. Spectrophotometric stydy of the new 1H-benzimidazole-2-yl hydrazones on iron induced oxidative damage in model systems containing lecithin and deoxyribose

The effect of the tested new 1*H*-benzimidazole-2-yl hydrazones from series B on iron induced lecithin oxidative damage is presented in Figure 17A. In the samples containing the reference compounds and all hydrazones, except for **5.26.**, administrated at concentration 90 μM, the absorbance values at 532 nm were lower compared to the controls. This indicates

decrease of the extent of molecular damage and well expressed protection effect against ferrous induced peroxidation. The estimated extent of molecular damage in the presence of quercetin was around 20%. In the samples containing mono-, di- and trimethoxyphenyl substituted hydrazones the observed extent of molecular damage was higher than 45%. The effect of the mono-methoxy hydrazone **5.21.** was statistically identical to those of the dimethoxy substituted derivatives **5.22.** and **5.23**. The modulation effect of **5.21.** was also comparable to the results for the hydrazone with mono hydroxyphenyl moiety **5.16.** The trimethoxy substituted hydrazone **5.24.** denoted more substantial protection compared to **5.21.** but it was still equivalent to the compounds **5.22.**, **5.25.** и **5.27.**. The di- and trihydroxy substituted hydrazones **5.17.**, **5.19.** и **5.20.** showed excellent protective effect – for **5.19.** и **5.20.** equal to the effect of quercetin.

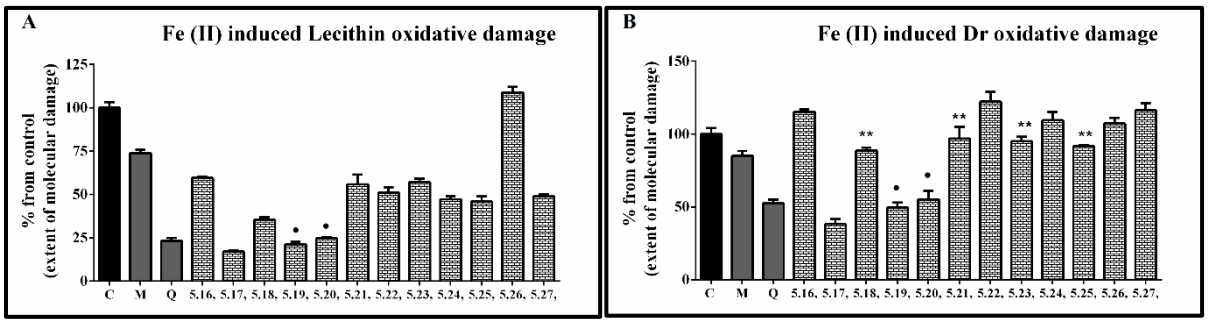

*Figure 17. Protection effects of compounds **5.16-5.27.** from series B on iron induced oxidative damage of biologically relevant molecules: (A) degree of molecular oxidative damage observed in lecithin containing model system and (B) degree of molecular oxidative damage observed in deoxyribose containing model system*

The ability of the compounds to protect the deoxyribose molecules from iron induced molecular degradation is shown at Figure 17B. In this system the tested benzimidazoles displayed both prooxidant and antioxidant effects depending on the molecular structure. The extent of the observed prooxidant effect was negligible to modest. The mono-, di- and trimethoxy substituted hydrazones either increased the absorbance values compared to the controls or did not exert any modulation effect. More substantial deoxyribose degradation and enhancement of the induced by iron molecular damage has been observed in the samples containing **5.16, 5.22.** and **5.27**. For all of these samples the estimated parameter was over 115%. As in the lecithin containing system, the derivatives possessing hydroxyl groups in vicinal positions in the phenyl ring were better molecular protectors under the conditions of ferrous iron induced peroxidation. Compounds **5.19.** and **5.20.** had equivalent effect to the reference quercetin and denoted extent of molecular damage close to 50%. The strongest protection effect was observed with the samples containing **5.17.** which exerted extent of molecular damage lower than 40% – considerably better protection effect compared to both reference compounds.

The performed assay denoted a higher radical scavenging ability of the hydroxyl substituted 1*H*-benzimidazole-2-yl hydrazones than other earlier studied benzimidazole derivatives as for example benzimidazoles containing N-methyl-1,3,4-thiadiazol-2-amine and 4-methyl-2H-1,2,4-triazole-3(4H)-thione moieties, 2-amino- and 5-aryl-1,3,4-oxadiazole moieties moieties and N,N-disubstituted benzimidazole-2-thione hydrazine derivatives. On the other side, taking into account the comparison to the reference compounds used in the experiments, it could be concluded that the observed effects of the hydroxyl substituted 1*H*-benzimidazole-2-yl hydrazones are close to those of catechin and flavonol compounds and superior to melatonin derivatives.

The study of the oxidative damage to biologically relevant molecules, the reference compounds and most of the benzimidazolyl hydrazones showed absorbance values at 532 nm lower than the control samples. There was a reduction in the extent of molecular damage and a protective effect against iron-induced peroxidation.

In the system containing lecithin a group of eight hydrazones (**5.28, 5.33-5.39**) from series C exhibited a statistically identical protective effect (Figure 18A). The presence of one or more methoxyl groups in the phenyl fragment leads to a moderate and good effect, but the introduction of an additional hydroxyl group does not lead to enhancement of the protective effect. Hydrazones that contain two hydroxyl groups (at *ortho*- and *meta*/*para*-position) showed the highest ability to protect the cell from induced lipid peroxidation.

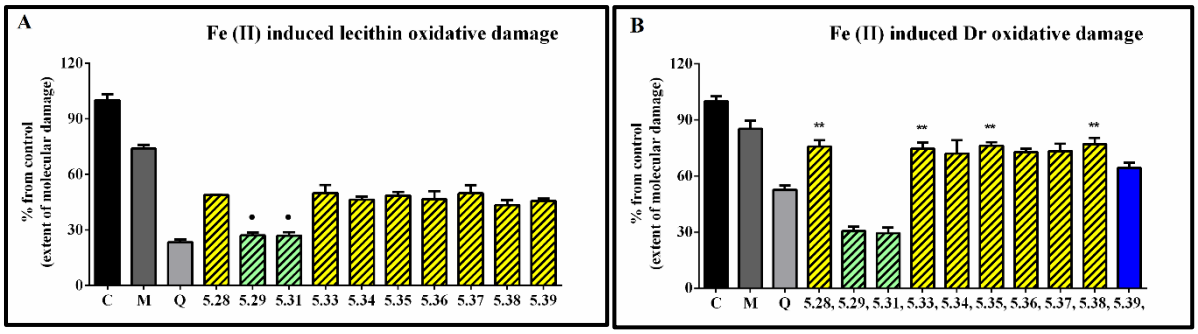

*Figure 18. Protection effects of compounds **5.28-5.39** on iron induced oxidative damage of biologically relevant molecules: (A) degree of molecular oxidative damage observed in lecithin (B) degree of molecular oxidative damage observed in deoxyribose*

According to the results for the deoxyribose-containing model system, seven compounds (**5.28, 5.33-5.38**) possessed an identical protective effect, comparable to that of melatonin (Figure 18B). Hydrazones **5.28** and **5.29** exhibited the most pronounced protective effect in the given system, better than the reference quarcetin and melatonin.

Comparing the structures of the synthesized benimidazolyl hydrazones and the modulating effect, it could be concluded that the presence of more than one hydroxyl group in the phenyl moiety is an essential factor affecting the ability of the tested hydrazones to neutralize stable free radicals and protect biologically important molecules. Their effect is close to that of the reference quercetin.

4. Computational study of the radical scavenging activity

At molecular level, the studied hydrazones could exert their radical scavenging activity through several probable mechanisms (Scheme 6). The first one of them comprises direct hydrogen atom transfer from the antioxidant to the free radical (HAT mechanism). Another probable mechanisms are the two-steps reaction pathways where the electron and proton are transferred in separate steps from the antioxidant to the free radical: single electron transfer followed by proton transfer (SET-PT mechanism) and sequential proton loss electron transfer (SPLET mechanism). A fourth possible way for deactivation of the free radicals is radical adduct formation (RAF mechanism) where the antioxidant covalently binds to the free radical.

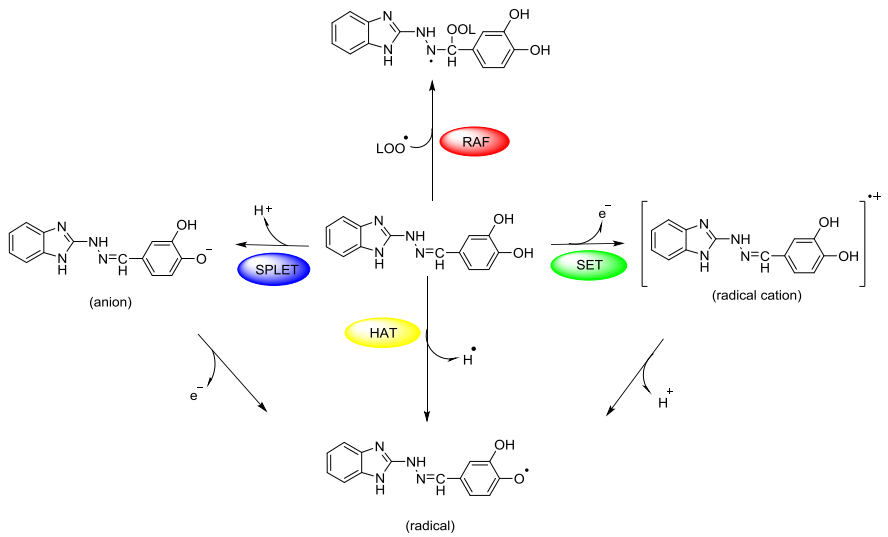

*Scheme 6. Probable mechanisms of radical-scavenging activity (compound **5.19**)*

In the same way, the molecular structure of the studied 1*H*-benzimidazole-2-yl hydrazones suggest several possible sites for hydrogen atom transfer, deprotonation and radical adduct formation. For instance, compound **5.19** might cleave the bonds N5-H10, N11-H24, O20-H22, O21-H23 and C13-H25 (for numbering cf. Scheme 7) in order to transfer a hydrogen atom or a proton as shown in blue in Scheme 7. Radical attack for adduct formation is also possible at several reaction sites: C1, C2, C4, C6 etc. (shown in red in Scheme 7). The reactivity for HAT of the above mentioned sites in compound **5.19** was estimated by calculating the respective bond dissociation enthalpies (BDE) resulting in the formation of radicals R1-R5 (Scheme 7). The most reactive site is denoted by the lowest enthalpy. It was previously demonstrated that DFT/B3LYP calculations are a good choice for estimation of the reaction enthalpies as they can provide a fairly accurate agreement between the calculated values and the available experimental data as well as describe reliably the structure-activity relationship for antioxidants with diverse chemical structure at reasonable computational time. On the other hand, the use of at least double-zeta basis set, including polarization and diffuse functions, is recommended, therefore the B3LYP//6-311++G(d,p) combination was applied in the present calculations. The results obtained at this computational level allow a useful comparison with earlier studied antioxidants.

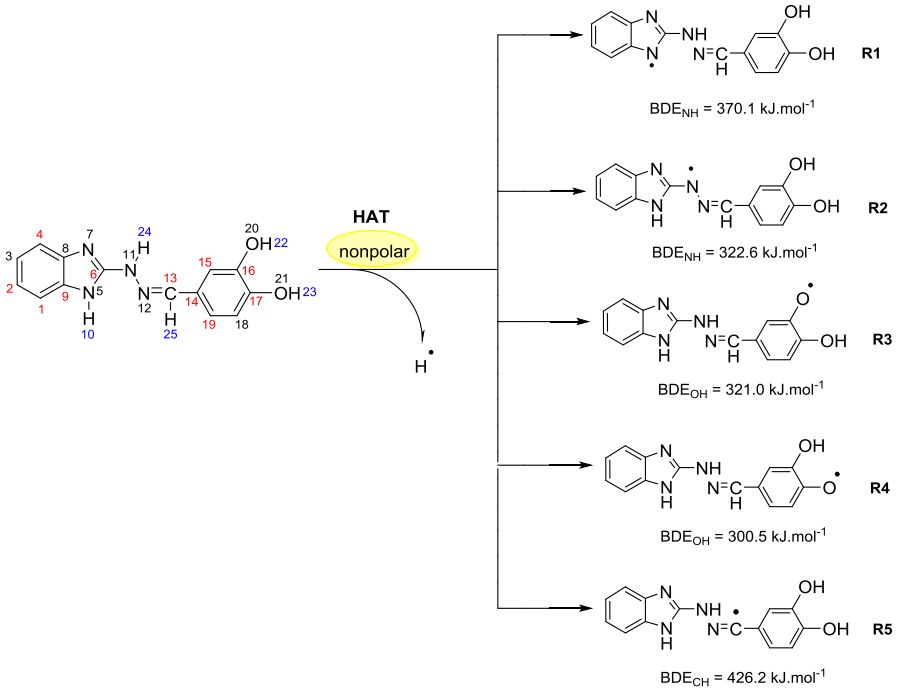

*Scheme 7. Possible sites for hydrogen atom transfer (in blue) and radical adduct formation (in red) for compound **5.19** along with the radicals formed by HAT and the respective bond dissociation enthalpies, calculated at B3LYP/6-311++G(d,p) level of theory in benzene*

The calculations in gas phase and benzene medium outlined the hydroxyl group at *para* position in the phenyl ring as the most active one (BDE in benzene 300.5 kJ.mol^{-1}; BDE in gas phase 293.2 kJ.mol^{-1}), followed by the hydroxyl group at *metha* position in the phenyl ring (BDE in benzene 321.0 kJ.mol^{-1}; BDE in gas phase 313.4 kJ.mol^{-1}) and the amino group in the hydrazine chain (BDE in benzene 322.6 kJ.mol^{-1}; BDE in gas phase 316.5 kJ.mol^{-1}). Moreover, the calculated BDE values are close to the calculated BDE values of known phenolic antioxidants such as α-tocopherol (BDE in gas phase 297 kJ.mol^{-1}, calculated at the same level of theory) and quercetin (with lowest O-H BDE value estimated to 305 kJ.mol^{-1} at the same level of theory).

The amino group in the benzimidazolyl fragment and the C-H bond from the azomethine group of compound **5.19** are characterized by a much lower reactivity (with BDE values 370.1 (BDE in gas phase 366.7 kJ.mol^{-1}) and 426.2 kJ.mol^{-1} (BDE in gas phase 418.7 kJ.mol^{-1}), thus not expected to contribute significantly to the radical scavenging properties of the compound. For comparison, the BDE of the indolyl N-H bond in melatonin and the methylene group next to the indolyl fragment were also calculated. The first one is 355 kJ.mol^{-1}, whereas the latter - 428 kJ.mol^{-1}, respectively.

The radical scavenging ability of the antioxidants is related to the stability of the formed radicals, which on turn is affected by the delocalization of the unpaired electron over the conjugated system. In order to estimate the stability of R4, R3 and R2 radicals of **5.19**, the spin density distribution was examined and compared (Figure 19).

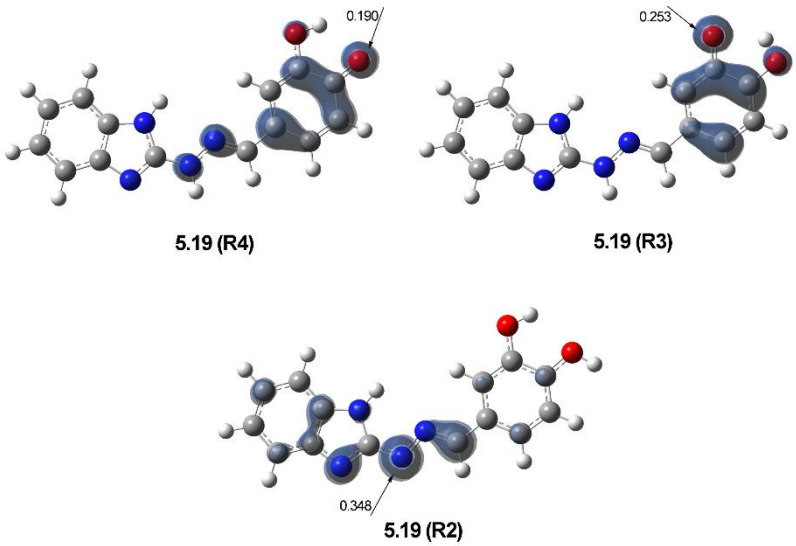

*Figure 19. Visualisation of spin density of the three most stable radicals **R4**, **R3** and **R2** of **5.19**, calculated at B3LYP/6-311++G(d,p) level of theory in benzene*

Radical **R4** showed the highest delocalization of spin density – only 0.176 of the unpaired electron are found on O21, while the greater part of it is spread over the phenyl ring and the hydrazone chain. In radical **R3** the spin density is delocalized only over the phenyl ring with 0.231 e^- localized on O20, while in radical **R2** it is limited within the hydrazone chain and part of the benzimidazole ring, with 0.311 e^- localized on N11. These data indicate **R4** as the most stable radical, followed by **R3** and **R2**. The order of stability of radicals **R4**, **R3** and **R2**, correspond to the order of reactivity at the different reaction sites established by the calculated BDE values. Such correlation between the two parameters has been previously discussed for other phenolic antioxidants.

Further the reaction enthalpies for HAT, SET-PT and SPLET mechanisms of all hydrazones **5.16-5.27.** from series B were computed in gas phase and water. The ability to deactivate free radical via HAT mechanism was described by the BDE values. The ionization potentials (IP) were used to describe the ability of the compounds to transfer a single electron via SET-PT mechanism, while the proton affinities (PA) were used to estimate the ability to transfer a proton via SPLET. Based on the comparison of the BDE values to IPs and PAs, it is possible to judge which mechanism is expected to govern the antioxidant action of the studied compounds. The lower the reaction enthalpy, the more easily would be followed the particular reaction pathway. On the other hand, the comparison of the reaction enthalpies of the different compounds might clarify the relationship between the molecular structure and the experimentally determined radical scavenging activity. The reaction enthalpies for each compound were modelled at all possible reaction sites. Figure 20a presents the lowest BDEs, IPs and PAs found for all compounds in gas phase. As it could be seen the IP and PA values lay far above the respective BDE values for all studied compounds (Figure 20a), pointing out that the SET-PT and SPLET mechanism require significantly more energy than HAT and therefore are not likely to occur in nonpolar phase.

It was established that for compounds **5.19.** and **5.27.**, bearing hydroxyl groups in 3 and 4 position of the phenyl ring, the lowest BDE corresponds to the cleavage of one of the O-H bonds and are 293.21 and 314.49 $kJ.mol^{-1}$, correspondingly. For compounds **5.21-5.24.**, where only methoxyl groups are present in the phenyl ring, the lowest BDEs are connected to the cleavage of the N5-H10 bond from the benzimidazole fragment. Correspondingly they

are higher than the O-H BDE values of **5.18-5.20.** and range from 315.24 to 373.81 kJ.mol^{-1}. For all derivatives containing hydroxyl groups in 2-position of the phenyl ring the lowest BDE are connected to the cleavage of the N5-H10 bond similarly to **5.21-5.24.**. It should be noted that the compounds bearing vicinal hydroxyl groups *i.e.* **5.17-5.20** possess the lowest BDEs within the whole studied series and the 3,4-dihydroxyl derivative **5.19.** is outlined as the most active one with BDE of 293.21 kJ.mol^{-1}. Based on that, it is expected to be the most active via HAT mechanism in nonpolar medium.

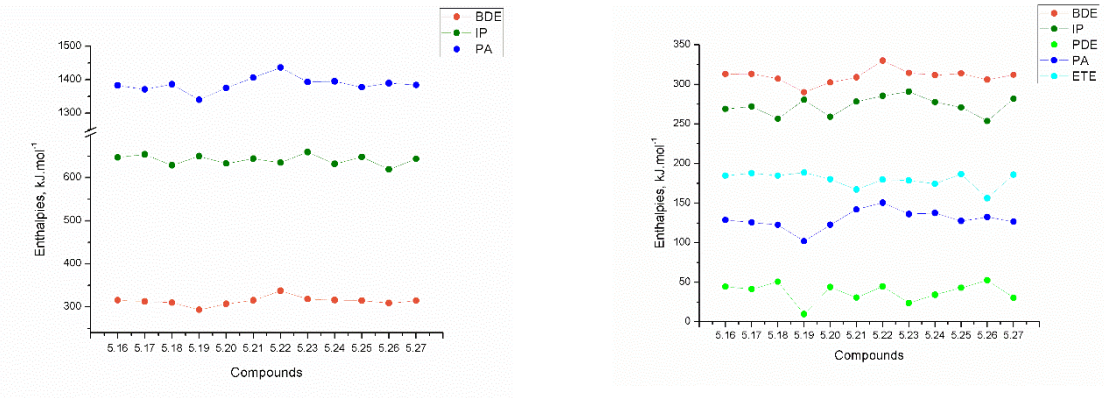

(a) (b)

*Figure 20. Reaction enthalpies for compounds **5.16-5.27** from series B in gas phase (a) and water (b): dissociation enthalpy (BDE), ionization potential (IP), proton dissociation enthalpy (PDE), proton affinity (PA), and electron transfer enthalpy (ETE), calculated at B3LYP/6-311++G** level of theory*

In water the BDE values of compounds **5.16-5.27** from series B are slightly lowered in comparison to the gas phase ones (they vary in the range 291.75-330.01 kJ.mol^{-1}), but follow the same trend (Figure 20b). On the other hand, the calculated O-H and N-H proton affinities of **5.16-5.27.** in water are much lower than the respective BDEs showing that in polar medium the first step (deprotonation) of SPLET mechanism is favored over HAT. The PAs are connected to the same functional groups as in the HAT process. PAs are between 108.30 and 150.47 kJ.mol^{-1} – the lowest values were found again for the compounds bearing vicinal hydroxyl groups **5.17-5.20.**, and particularly for the 3,4-dihydroxyl derivative **5.19.** The second step (electron transfer) of the SPLET mechanism, described by the electron transfer enthalpy (ETE), also requires lower energy than the homolytic cleavage of the O-H or N-H bond for all studied compounds. The ionization potentials of **5.16-5.27.** in water are lower than the BDEs, but still higher than the PA values which indicate that the SET-PT mechanism is less probable than the SPLET in polar medium.

Summarizing the data in polar medium, it could be concluded that in this case SPLET is regarded as the most probable mechanism of antioxidant action and the derivatives with vicinal hydroxyl groups are expected again to show the highest activity. These results are in good agreement with the experimentally determined radical scavenging effects in DPPH, lecithin and deoxyribose assays, where the hydroxyl substituted hydrazones demonstrated the most potent radical scavenging effect. The presence of a phenyl fragment with vicinal hydroxyl groups has been associated to improved radical scavenging properties due to its conversion to *ortho*-quinone intermediates.

The ability of the studied compounds to deactivate different free radicals were modeled by transition states involving attack by $^{\bullet}OCH_3$, $^{\bullet}OOH$ and $^{\bullet}OOCH_3$, at all reactive sites identified in the preceding computational study. The calculations were carried out with compound **5.19** at SP M06-2X/6-311++G** level of theory. M06-2X/6-311++G** was selected

for the computations taking into account the reliability of this method for transition state studies. The activation energies ($\Delta G^{\ddagger}$) for all studied transition states in gas phase and solvent (water and benzene) for all three attacking radicals are presented in Table 5.

*Table 5. Gibbs free energies of activation ($\Delta G^{\ddagger}$) for the formation of transition states (TSs) of compound **5.19** with various free radicals corresponding to HAT mechanism, at 25°C , in kJ.mol^{-1}*

TSs	$\Delta G^{\ddagger}$ ((U)M06-2X/6-311++G**//(U)B3LYP/6-311++G**)								
	$^{\bullet}OCH_3$			$^{\bullet}OOH$			$^{\bullet}OOCH_3$		
	Gas phase	Water	Benzene	Gas phase	Water	Benzene	Gas phase	Water	Benzene
TS H10	67.64	69.23	77.44	90.83	81.24	90.59	95.07	86.47	97.32
TS H24	33.15	89.83	-	64.81	77.91	74.32	74.46	82.93	84.91
TS H22	-	18.08	-	75.71	81.95	86.09	80.93	81.31	90.32
TS H23	-	18.30	-	68.97	83.31	74.56	71.73	83.13	67.47
TS H25	71.01	83.94	79.93	115.15	125.92	122.74	119.82	132.74	128.83

The most stable transition states **TS H24**, **TS H22** and **TS H23** correspond to the formation of the most stable radicals **R2**, **R3** and **R4** for all attacking species. Unfortunately, we could not locate transition states between **5.19** and $^{\bullet}OCH_3$ for **TS H24** in benzene and **TS H22 and TS H23** in gas phase and benzene. The scans made (**5.19**)-O···H···O-CH_3 for **TS H22**'s and **TS H23**'s and (**5.19**)-N···H···O-CH_3 for **TS H24** do not indicate maximum in the energies corresponding to transition state. Having in mind the activation energies for **TS H22 ($^{\bullet}OCH_3$)** and **TS H23 ($^{\bullet}OCH_3$)** in water (around 18 kJ.mol^{-1} only) and the activation energies of the TS's for the other attacking radicals (values in gas phase and benzene lower than in water), it seems that the not detected TS's should have lower than 18 kJ.mol^{-1} activation energy. The optimized structures of the most stable TS's (Figure 21) show similarity in regard to the bond distances (in Å) for the breaking of O···H and N···H and forming new H···O bonds with the different free radicals. The distances in **TS H24**'s are longer compared to the other two transition states (**TS H23** and **TS H22)** for the same attacking free radical.

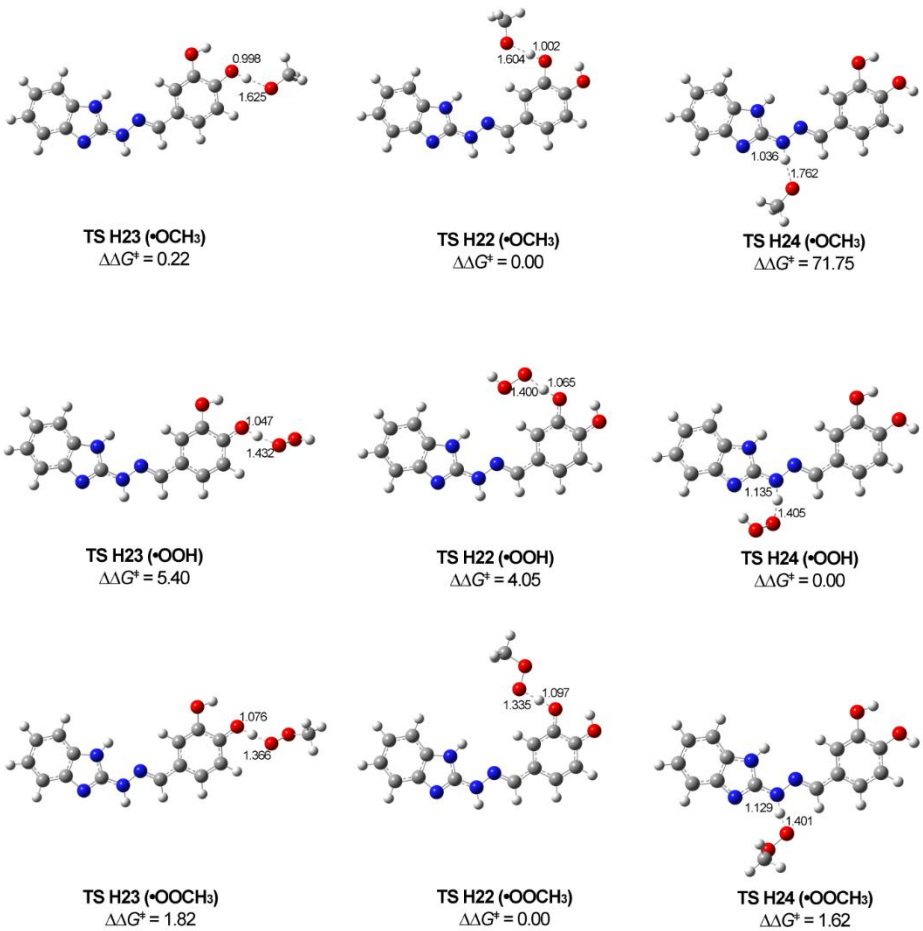

*Figure 21. Optimized structures of the TSs for the most stable radicals **R2**, **R3** and **R4** of **5.19** corresponding to the HAT mechanism. $\Delta\Delta G^{\ddagger}$ shows the difference in the activation energies between the TSs for every one of the studied radicals. Calculations are done on SP M06-2X/6-311++G** method in solvent water*

According to our theoretical study, the radical scavenging can go through RAF mechanism as well. The calculations showed that the most stable transition states (TS) between the studied radicals and **5.19** are at C13 position (Table 6).

*Table 6. Gibbs free energies of activation ($\Delta G^{\ddagger}$) for the formation of transition states (TSs) of compound **5.19** with various free radicals corresponding to RAF mechanism, at 25°C, in kJ.mol^{-1}*

TSs	$\Delta G^{\ddagger}$((U)M06-2X/6-311++G**//(U)B3LYP/6-311++G**)								
	$^{\bullet}OCH_3$			$^{\bullet}OOH$			$^{\bullet}OOCH_3$		
	Gas phase	Water	Benzene	Gas phase	Water	Benzene	Gas phase	Water	Benzene
TS C1	68.15	74.93	75.89	102.16	104.87	107.80	115.53	119.58	122.07
TS C2	70.23	72.73	74.54	101.96	100.35	107.29	115.26	114.57	119.53
TS C4	72.23	71.69	75.85	102.99	100.31	107.88	117.04	116.04	121.04
TS C6	83.64	92.37	91.53	101.62	109.66	109.84	107.90	118.34	116.40
TS C9	73.18	78.53	80.13	107.77	107.56	112.57	121.37	121.36	126.40
TS C13	52.87	60.20	59.55	73.13	82.25	80.70	80.72	91.13	88.93
TS C14	82.30	83.24	87.81	113.28	114.10	117.98	125.51	127.23	130.16
TS C15	70.08	70.10	76.12	102.25	101.91	107.36	112.21	113.95	117.81
TS C16	70.29	72.34	82.25	107.55	101.44	108.84	117.23	115.83	121.77
TS C17	47.72	61.16	57.31	83.81	91.66	91.33	95.10	104.29	102.26
TS C19	65.02	70.42	71.00	94.11	97.89	98.95	106.31	112.12	112.56

The optimized geometries of the possible transition states involved in the RAF mechanism are shown in Figure 22. The most relevant parameter is the C···O distance corresponding to the forming new bond and it was found to be around 2 Å for all calculated TS's.

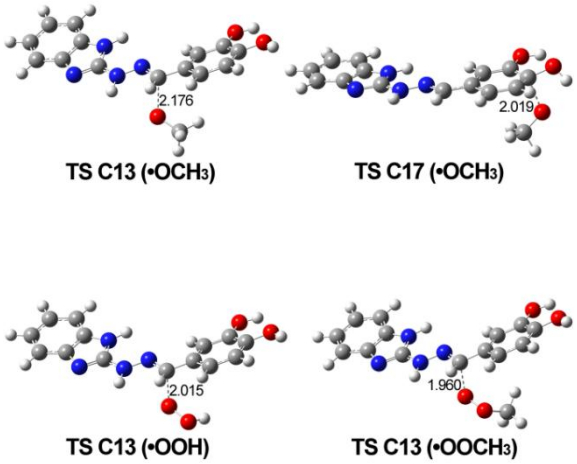

*Figure 22. Optimized structures of the most probable TSs of **5.19** corresponding to the RAF mechanism for every one of the studied radicals. Calculations are done in solvent water*

The values of ($\Delta G_{reaction}$) in Table 7 for this mechanism showed that concerning the $^{\bullet}OCH_3$, the reaction can proceed at C13 and C17 position in **5.19** in water and benzene; when the radical is $^{\bullet}OOH$, the reaction still will be possible at C13 (water and benzene), while when the reacting species is $^{\bullet}OOCH_3$, the reaction will follow this mechanism with difficulty. Hypothetically, the RAF mechanism can occur to N12 (Scheme 7) as well, but any attempt to locate the corresponding products and transition states brought us failure.

*Table 7. Gibbs Free Energies of Reaction ($\Delta G_{reaction}$) corresponding to hydrogen atom transfer (HAT) and radical adducts formation (RAF) of compound **5.19** with various free radicals, at 25°C, in kJ.mol^{-1}, with respect to the isolated reactants*

Позиция за атака	$\Delta G_{reaction}$((U)M06-2X/6-311++G**//(U)B3LYP/6-311++G**)								
	$^{\bullet}OCH_3$			$^{\bullet}OOH$			$^{\bullet}OOCH_3$		
	Gas phase	Water	Benzene	Gas phase	Water	Benzene	Gas phase	Water	Benzene
					HAT				
H10	-36.36	-46.88	-37.65	34.50	23.15	32.96	40.00	30.75	39.62
H24	-84.27	-87.42	-82.32	-13.41	-17.39	-11.71	-7.91	-9.79	-5.05
H22	-84.32	-84.46	-83.50	-13.46	-14.43	-12.89	-7.96	-6.83	-6.23
H23	-99.63	-99.29	-98.46	-28.77	-29.26	-27.85	-23.27	-21.66	-21.20
H25	3.36	2.21	5.44	74.22	72.24	76.05	79.71	79.84	82.70
					RAF				
C13	-72.93	-59.30	-63.33	-12.69	2.89	-1.05	-1.74	14.23	7.63
C17	-33.50	-20.52	-24.00	33.22	43.65	41.08	43.15	54.25	51.38
C19	-7.15	3.53	0.05	49.64	57.48	56.23	61.73	69.46	67.33
C6	-7.44	6.19	2.97	46.14	59.22	55.08	59.45	73.11	69.60
C15	-0.32	6.64	6.26	55.90	61.67	62.62	66.13	71.97	72.00
C1	5.92	16.26	13.97	63.08	70.87	70.68	76.25	84.87	83.93
C2	12.27	20.53	19.17	67.01	70.94	72.33	80.20	85.44	87.28
C4	3.91	10.93	11.13	61.61	63.63	66.99	72.86	75.68	79.21
C9	32.02	42.70	40.60	91.60	96.73	98.32	106.09	110.98	112.45
C14	31.47	37.22	37.58	87.01	92.49	91.45	98.65	103.71	106.64
C16	4.70	8.28	11.17	68.99	69.92	73.65	80.22	81.57	86.95

Having in mind the values of $\Delta G_{reaction}$ and $\Delta G^{\ddagger}$ for the TSs of HAT and RAF mechanisms, the reaction between $^{\bullet}OCH_3$ and **5.19** will go mainly through HAT mechanism at H23, H22 and H24 position.

When the reacting species is $^{\bullet}OOH$ both mechanisms (HAT and RAF) can be followed: HAT – at H23, H22 and H24, and RAF - at C13 position. The most stable TSs for HAT and RAF mechanism have similar values of $\Delta G^{\ddagger}$ (HAT: H24 – 77.91 (water) and 74.32 (benzene) kJ.mol^{-1} and RAF: C13 – 82.25 (water) and 80.70 (benzene) kJ.mol^{-1}).

The $^{\bullet}OOCH_3$ could be deactivated only by HAT mechanism. The calculations showed a lower reactivity of the radical compared with the other two studied radicals. According to the $\Delta G_{reaction}$, the reactions are slightly exothermic and in the same time the $\Delta G^{\ddagger}$ of the most stable TSs are higher than the $\Delta G^{\ddagger}$ of the other two radicals at the respective positions.

All gathered computational data demonstrated that the newly synthesized 1*H*-benzimidazole-2-yl hydrazones possess very versatile radical scavenging properties – several reaction sites characterized by relatively low reaction enthalpies and possibility to act simultaneously through several possible reaction pathways. It was also found that the predicted activities of the compounds from series B are in good correlation with the experimentally observed antiradical activity.

The ability of the synthesized hydrazones from series C to exert the radical-scavenging activity and the possible mechanisms of antioxidant activity were also studied by quantum-chemical calculations.

As in the series B, there are several possible sites for hydrogen atom transfer, deprotonation and radical adduct formation such as bonds N5-H10, N11-H24, O20-H22, O21-H23 and C13-H25 for hydrazone **5.31** (for numbering cf. Scheme 8). HAT mechanism was characterized by bond dissociation enthalpy (BDE) for the radicals R1-R5 (Scheme 8).

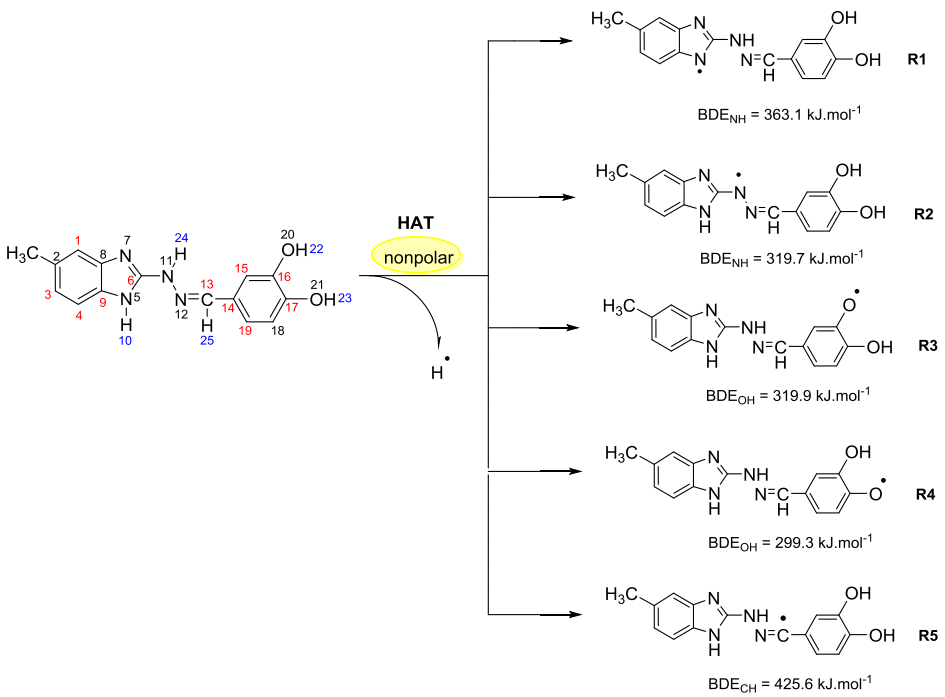

*Scheme 8. Possible sites for hydrogen atom transfer (in blue) and radical adduct formation (in red) for compound **5.31** along with the radicals formed by HAT and the respective bond dissociation enthalpies, calculated at B3LYP/6-311++G(d,p) level of theory in benzene*

The data from the calculations in gas phase and benzene supported the trends found for the analogue from series B, and outlined the hydroxyl group at *para*-position in the phenyl

moiety (bond O21-H23) as the most reactive. The lowest value of BDE corresponds to the formation of radical **R4** (BDE in benzene 299.3 kJ.mol^{-1}; BDE in gas phase 292.3 kJ.mol^{-1}). Radicals **R2** (BDE in benzene 319.7 kJ.mol^{-1}; BDE in gas phase 314.6 kJ.mol^{-1}) and **R3** (BDE in benzene 319.9 kJ.mol^{-1}; BDE in gas phase 312.8 kJ.mol^{-1}) are the next that might form. On the other hand, the N5-H10 and C13-H25 bonds corresponding to the amino group of the benzimidazole heterocycle and the C-H bond from the azomethine chain possesses the lowest activity according to the BDE values: N5-H10 - BDE in benzene 363.1 kJ.mol^{-1}; BDE in gas phase 360.7 kJ.mol^{-1} and for the C13-H25 - BDE in benzene 425.6 kJ.mol^{-1}; BDE in gas phase 418.7 kJ.mol^{-1}.

In addition, the delocalization of the unpaired electron over the obtained radicals **R4**, **R3** and **R2** was studied, which is crucial for the stability and activity towards free radicals. The results from the spin density are presented for hydrazone **5.31.** in the following Figure 23.

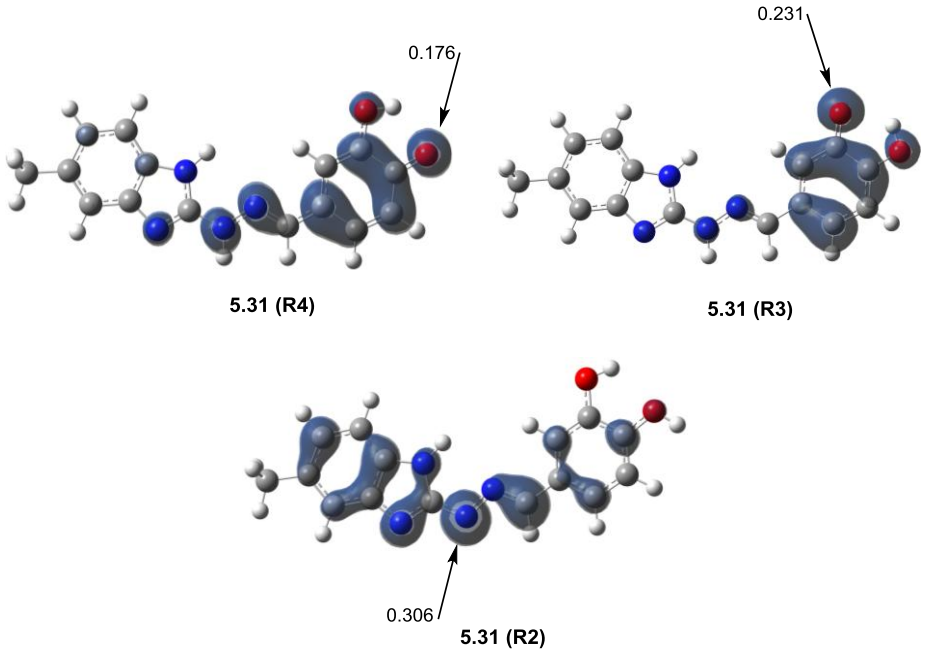

*Figure 23. Visualisation of spin density of the three most stable radicals **R4**, **R3** and **R2** of **5.31**, calculated at B3LYP/6-311++G(d,p) level of theory in benzene*

Radical **R4** showed the highest delocalization of spin density as only 0.176 of the unpaired electron is found on the oxygen atom O21 and the rest is delocalized over the phenyl fragment and the hydrazone chain. In radical **R3** 0.231 of the unpaired electron is localized on O20 (the hydroxyl group at the 3-position) and the rest of the spin density is spred on the phenyl residue. For radical **R2** it could be summarized that most of the spin density is concentrated on the benzimidazole heterocycle and the hydrazone chain with 0.306 e^{-} on N11 of the amino group. Similar to the conclusions for series B, radical **R4** is the most stable in this case, followed by **R3** and **R2**.

For better understanding the antioxidant mechanisms, the reaction enthalpies for all derivatives from series C were calculated in gas phase and water. The values of BDE, IP and PA enthalpies in gas phase were compared in order to clarify which mechanism (HAT, SET-PT or SPLET) is favored in nonpolar medium. The results are presented in Figure 24a. It is noteworthy that the values for IP and PA are higher compared to those for BDE, i.e. the HAT mechanism is preferred in a non-polar medium (gas phase).

Compounds **5.31**, **5.39** and **5.40** which contain hydroxyl groups at *meta* and *para*-position in the phenyl core have the lowest BDE values (292.37 kJ.mol^{-1}, 315.21 kJ.mol^{-1} and 311.94 kJ.mol^{-1}) corresponding to the homolytic cleavage of one of the bonds O20-H22 or O21-H23. For the methoxy derivatives **5.33-5.36**, the radical with the lowest BDE value (311.69-334.17 kJ.mol^{-1}) was obtained based on the hydrogen transfer from the amino group of the benzimidazole heterocycle. The hydrazones containing hydroxyl groups at *ortho* position in the aromatic residue (**5.28-5.30; 5.32; 5.37-5.38**), the BDE was derived by dissociation of the amino group from the benzimidazole fragment.

Compound **5.31** possessed the lowest BDE, i.e. according to the theoretical calculations this hydrazone has the most prominent radical-scavenging activity, which proceeds by HAT mechanism in a nonpolar environment. The presence of a methyl group at the 5(6)-position in the benzimidazole fragment did not affect the radical-scavenging activity based on the calculations.

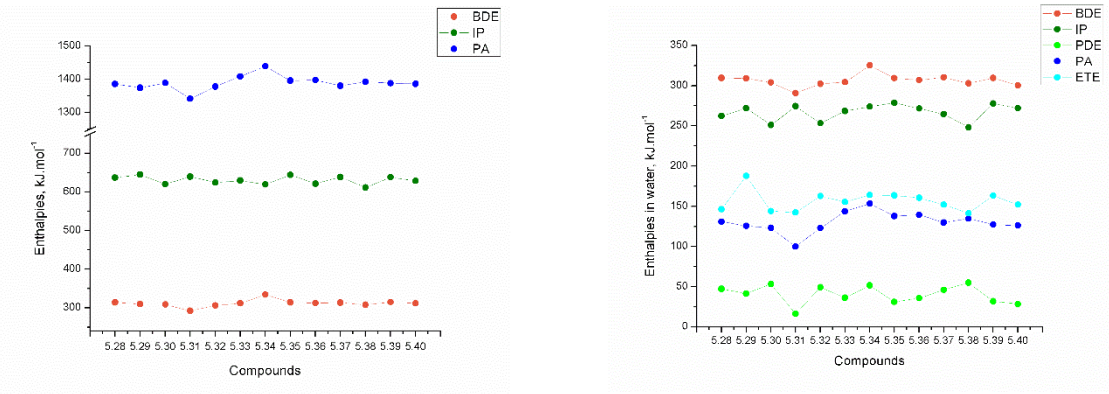

(a) (b)

*Figure 24. Reaction enthalpies for compounds **5.28-5.40** in gas phase (a) and water (b): dissociation enthalpy (BDE), ionization potential (IP), proton dissociation enthalpy (PDE), proton affinity (PA), and electron transfer enthalpy (ETE), calculated at B3LYP/6-311++G** level of theory*

On the other hand, in polar medium (water), the BDE values for all benzimidazolyl hydrazones from series C had higher values than the other enthalpies (ranged from 290.61-325.32 kJ.mol^{-1}), which suggests that in water HAT mechanism is not energetically favoured (Figure 24b). The SPLET mechanism is characterized by proton affinity (PA) and electron transfer enthalpy (ETE), whose values are lower than BDE, i.e., in water medium, based on the obtained data for PA, it could be concluded that deprotonation is the preferred reaction. The obtained PA enthalpies regarding the participating functional groups follow the established trends for HAT mechanism and the values are in the range 99.90-139.43 kJ.mol^{-1} for all hydrazones of series C. Hydrazone **5.31** has the lowest value of PA-99.90 kJ.mol^{-1}. The IPs characterizing the SET-PT mechanism are higher than those of PA (ranging from 248.21 to 277.89 kJ.mol^{-1}), i.e. SPLET is the most probable in polar medium compared to SET-PT and HAT mechanisms.

The ability of the studied compounds to deactivate different free radicals were modeled by transition states of **5.31.** involving attack by $^{\bullet}OCH_3$, $^{\bullet}OOH$ and $^{\bullet}OOCH_3$, at all reactive sites at (SP) (U)M06-2X/6-311++G**//(U)B3LYP/6-311++G**) level of theory. The activation energies ($\Delta G^{\ddagger}$) for all studied transition states in gas phase and solvent (water and benzene) for all three attacking radicals are presented in Table 8.

*Table 8. Gibbs free energies of activation ($\Delta G^{\ddagger}$) for the formation of transition states (TSs) of compound **5.31** with various free radicals corresponding to HAT mechanism, at 25°C, in kJ.mol^{-1}*

TSs	$\Delta G^{\ddagger}$ ((U)M06-2X/6-311++G**//(U)B3LYP/6-311++G**)								
	$^{\bullet}OCH_3$			$^{\bullet}OOH$			$^{\bullet}OOCH_3$		
	Gas phase	Water	Benzene	Gas phase	Water	Benzene	Gas phase	Water	Benzene
H10	66.26	68.85	72.82	86.70	77.28	81.94	90.84	83.22	89.12
H24	-	-	-	62.64	75.59	67.98	72.63	82.24	78.87
H22	-	16.74	-	75.54	80.80	82.33	80.49	80.06	87.88
H23	-	18.53	-	91.11	84.11	92.21	71.26	81.99	70.68
H25	71.77	85.46	76.53	115.26	126.67	118.51	119.51	133.59	125.12

The transition states for positions H24 (all solvents), H22 (gas phase and benzene) and H23 (gas phase and benzene) between hydrazone **5.31.** and attacking radical •OCH3, could not be detected due to the lower energy. The most stable transition states TS H24, TS H22 and TS H23 correspond to the most stable radicals **R2**, **R3** and **R4** formed by HAT mechanism (Figure 25), for all attacking radicals. The optimized structures of the most stable transition states of **5.31.** and bond distances (in Å) are illustrated in Figure 25.

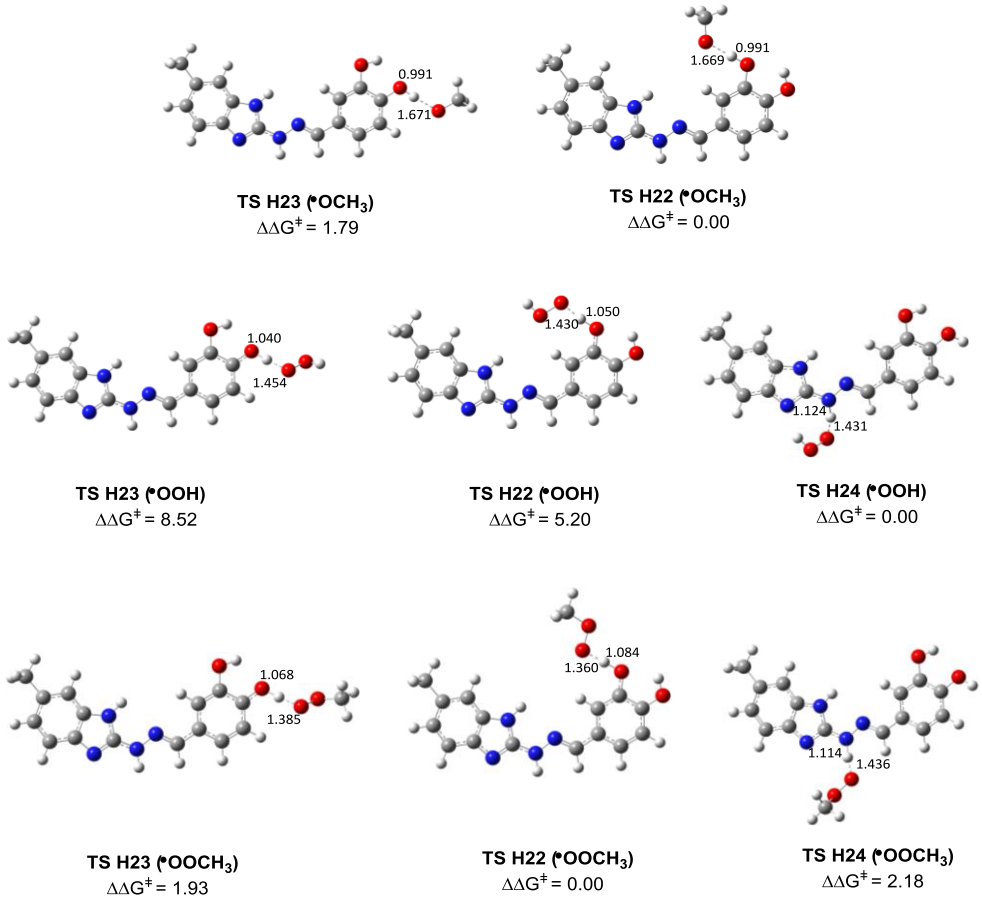

*Figure 25. Optimized structures of the TSs for the most stable radicals **R2**, **R3** and **R4** of **5.31.** corresponding to the HAT mechanism. $\Delta\Delta G^{\ddagger}$ shows the difference in the activation energies between the TSs for every one of the studied radicals. Calculations are done on SP M06-2X/6-311++G** method in solvent water*

According to the theoretical study, the most stable transition states could be formed at position C13 (the carbon atom of the double azomethine bond) of the hydrazone for all attacking radicals. The values of the Gibbs free energies of activation for this position vary in

the interval 52.45-91.18 kJ.mol^{-1}. However, in gas phase and water the most stable transition states between •OCH3 radical and hydrazone **5.31.** were obtained at C17 position (the carbon atom at the OH group in the *para*-position) with values of 46.56 (gas phase) and 52.48 (benzene) (Table 9).

*Table 9. Gibbs free energies of activation ($\Delta G^{\ddagger}$) for the formation of transition states (TSs) of compound **5.31** with various free radicals corresponding to RAF mechanism, at 25°C, in kJ.mol^{-1}*

TSs	$\Delta G^{\ddagger}$((U)M06-2X/6-311++G**//(U)B3LYP/6-311++G**)								
	$^{\bullet}OCH_3$			$^{\bullet}OOH$			$^{\bullet}OOCH_3$		
	Gas phase	Water	Benzene	Gas phase	Water	Benzene	Gas phase	Water	Benzene
TS C1	62.03	69.43	63.70	96.43	100.20	97.36	109.08	113.78	111.41
TS C2	64.73	70.61	67.68	95.85	94.59	95.74	109.32	107.29	108.68
TS C4	72.35	72.15	71.41	103.23	100.21	103.63	116.10	115.76	116.23
TS C6	80.52	88.89	84.02	97.33	105.82	100.49	103.60	114.01	108.68
TS C9	72.12	77.83	75.14	106.84	106.39	107.46	119.55	119.96	120.47
TS C13	52.45	60.29	54.32	72.32	81.96	75.14	79.93	91.18	84.18
TS C14	81.35	82.58	84.25	113.33	112.64	113.33	125.83	125.32	126.64
TS C15	70.59	71.60	71.37	101.99	101.92	102.29	111.71	112.59	112.21
TS C16	69.54	69.51	71.43	107.07	103.00	104.46	116.53	114.38	115.33
TS C17	46.56	60.43	52.48	82.80	91.67	86.84	94.31	103.99	97.17
TS C19	64.28	68.85	66.10	93.12	96.62	94.16	105.51	111.95	108.05

The optimized geometries of the possible transition states involved in the RAF mechanism are shown in Figure 26.

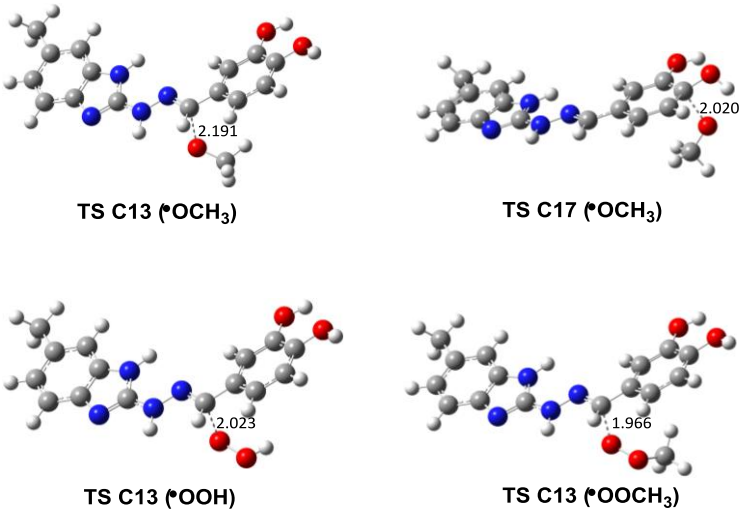

TS C13 ($^{\bullet}OCH_3$) **TS C17 ($^{\bullet}OCH_3$)**

TS C13 ($^{\bullet}OOH$) **TS C13 ($^{\bullet}OOCH_3$)**

*Figure 26. Optimized structures of the most probable TSs of **5.31.** corresponding to the RAF mechanism for every one of the studied radicals. Calculations are done in solvent water*

The values of $\Delta G_{reaction}$ presented in Table 10 for this mechanism showed that concerning the $^{\bullet}OCH_3$, the reaction can proceed at C13 and C17 position in **5.31** in water and benzene; when the radical is $^{\bullet}OOH$, the reaction still will be possible at C13 (gas phase and benzene), while when the reacting species is $^{\bullet}OOCH_3$, the reaction is not possible.

*Table 10. Gibbs Free Energies of Reaction ($\Delta G_{reaction}$) corresponding to hydrogen atom transfer (HAT) and radical adducts formation (RAF) of compound **5.31** with various free radicals, at 25°C, in kJ.mol^{-1}, with respect to the isolated reactants*

Позиция за атака	$\Delta G_{reaction}$((U)M06-2X/6-311++G**//(U)B3LYP/6-311++G**)								
	$^{\bullet}OCH_3$			$^{\bullet}OOH$			$^{\bullet}OOCH_3$		
	Gas	Water	Benzene	Gas	Water	Benzene	Gas	Water	Benzene

	phase			phase			phase		
					HAT				
H10	-41.67	-52.25	-47.12	29.19	17.77	23.49	34.69	25.38	30.15
H24	-87.48	-91.32	-90.03	-16.63	-21.29	-19.42	-11.13	-13.69	-12.76
H22	-86.14	-85.42	-88.10	-15.28	-15.39	-17.49	-9.78	-7.79	-10.83
H23	-100.31	-98.86	-100.57	-29.45	-28.83	-29.96	-23.96	-21.23	-23.30
H25	2.86	3.47	1.93	73.72	73.50	72.54	79.21	81.10	79.19
					RAF				
C1	-0.39	10.10	3.25	57.84	64.73	61.74	70.42	77.78	73.38
C2	5.60	15.19	8.90	59.56	65.30	61.95	72.85	79.82	76.64
C4	2.87	10.48	6.11	59.67	61.84	60.79	71.29	74.88	73.98
C6	-13.05	1.17	-6.80	40.30	53.68	44.95	53.20	67.15	58.64
C9	29.84	41.12	34.41	89.09	94.56	91.75	103.36	108.46	105.86
C13	-73.12	-59.15	-67.72	-13.17	2.30	-4.85	-2.26	14.72	3.77
C14	30.82	36.61	32.84	86.04	90.52	87.44	97.43	106.14	102.17
C15	-0.68	6.24	1.22	55.68	60.85	57.13	65.60	69.44	66.64
C16	5.04	10.19	7.73	69.68	70.04	70.36	78.90	82.59	82.68
C17	-34.47	-21.75	-28.95	31.88	42.81	35.84	41.25	53.22	45.93
C19	-8.69	2.40	-4.56	48.48	57.27	50.40	61.28	70.03	62.60

Considering the values of $\Delta G_{reaction}$ and $\Delta G^{\ddagger}$ for the TSs of HAT and RAF mechanisms, the reaction between $^{\bullet}OCH_3$ and **5.31** will go through both mechanisms HAT and RAF at H23, H22, H24 and C13 position. Nevertheless, the HAT mechanism is the preferred one.

When the reacting species is $^{\bullet}OOH$ both mechanisms (HAT and RAF) can be followed: HAT – at H23, H22 and H24, and RAF - at C13 position. The most stable TSs for HAT and RAF mechanism have similar values of $\Delta G^{\ddagger}$ (HAT: H24 – 75.59 (water) and 67.98 (benzene) $kJ.mol^{-1}$ and RAF: C13 – 81.96 (water) and 75.14 (benzene) $kJ.mol^{-1}$).

The $^{\bullet}OOCH_3$ could be deactivated only by HAT mechanism at H23, H22 and H24 positions. The calculations showed a lower reactivity of the radical compared with the other two studied radicals.

5. *Prediction of the physico-chemical properties and drug-likeness of the 1H-benzimidazol-2-yl hydrazones*

The data indicated that none of the benzmidazolyl-2-hydrazones from series A violates the rule of Lipinski. The molecular weights and the molecular volumes of the molecules are below 300 Daltons and 300 $Å^3$, respectively. The miLogP values (octanol/water partition coefficients), calculated as a sum of fragment-based contributions and correction factors according to the algorithm provided by Molinspiration, are less than 4 for all of them, which suggests an optimal absorption and oral bioavailability. The topological polar surface area (TPSA) i.e. the sum of the surface areas occupied by the oxygen and nitrogen atoms and the hydrogens attached to them, is another significant physico-chemical parameter characterizing the good bioavailability, transport properties, and drug absorption such as blood-brain penetration, and intestinal absorption. TPSA values below 140 $Å^2$ indicate that good intestinal absorption is expected for the new drug candidates, while TPSA values below 60 $Å^2$ – good blood-brain penetration. All hydrazones **5.1-5.15** are expected to have good intestinal absorption and compounds **5.1**-**5.6** satisfies also the criteria for good blood-brain penetration. The oral bioavailability and the efficient binding to receptors and channels, might be evaluated also by the number of the rotatable bonds (N_{rotb}) as measure of the molecular flexibility. Molecules with less than 10 rotatable bonds are recognized to have sufficient oral bioavailability. Hydrazones **5.6**, **5.9**, **5.10** and **5.14** show low number of

rotatable bonds – 6 or less. The benzimidazole moiety itself has no rotatable bonds and the hydrazone chain is also quite rigid as evidenced by the relatively large free energy differences between the DFT optimized conformers. On the other hand, **5.6**, **5.9**, **5.10** and **5.14** show good hydrogen-bonding capacity - 4-6 H-bond acceptors and 2 or 3 H-bond donors, which is beneficial for efficient binding to receptors and channels. Toxicological properties of the benzimidazole hydrazones were predicted by the OSIRIS Property explorer. The program provides an estimation of the mutagenic, irritant, tumorigenic and reproductivity risk. Most of the hydrazones show low mutagenic and irritant risk. Compounds **5.6**, **5.9**, **5.10** are predicted as compounds with low tumorigenic risk, and medium tumorigenic risk was found only for hydrazone **5.14**. According to the estimation, the presence of a methyl group in the benzimidazole moiety is related to a higher reproductivity risk than for the molecules without a substituent in the benzimidazole core.

Molinspiration tool predicts logP values less than 4 for all synthesized compounds from series B, thus suggesting good absorption and bioavailability. The topological polar surface area (TPSA) is below 140 $Å^2$ for all synthesized hydrazones according to Molinspiration so they are expected to exhibit good intestinal absorption. Compounds **5.21-5.23** and **5.16** with values 62-73 $Å^2$ approach the limit for blood-brain barrier penetration (below 60 $Å^2$). Hydrazones **5.16-5.19**, **5.22-5.24** and **5.25-5.27** show low number of rotatable bonds (N_{rotb}) – 6 or less consistent with sufficient oral bioavailability. All 1*H*-benzimidazole-2-yl hydrazones show good hydrogen-bonding capacity with 5-7 H-bond acceptors and 2 to 5 H-bond donors which is beneficial for efficient binding to biological targets. The estimation of the toxicological properties of the compounds was elucidated by OSIRIS Property explorer. All of the synthesized hydrazones are expected to show low tumorigenic risk. Most of the compounds are expected to exhibit low mutagenic risk as well. Only the presence of a hydroxy or methoxy group at the *metha*-position in the phenyl ring of hydrazones **5.17** and **5.25** might lead to an increased mutagenic risk. The expected irritant and reproductive risk for most of the compounds is also low. Medium irritant risk is expected only for compound **5.25** and a higher reproductive risk – for its positional isomer **5.26**, respectively.

According to Molinspiration's results, there are no hydrazones from series C that violate Lipinski's rule. The logP values are less tham 4, suggesting optimal bioavailability. According to the TPSA parameter, the compounds exhibited good intestinal absorption, and hydrazone **5.33**, which contains a methoxy group at *para*-position, approach the limit for blood-brain barrier penetration with a TPSA value of 62 Å2. Another indicator of good bioavailability is the number of rotatable bonds and most of the hydrazones show less than 5 rotatable bonds. The number of donors and acceptors of hydrogen bonds are 5-7 and 2-5, respectively. The studied derivatives from series C show a low tumorigenic risk. Compounds **5.29** and **5.37** exhibit a high mutagenic risk, and hydrazone **5.37** a medium irritant risk, which is due to the same structural modifications as in the compounds of series B. The presence of a methyl group in the benzimidazole fragment leads to high reproductive risk.

The results from SwissADME software suggest that all synthesized hydrazones of series A have excellent gastrointestinal absorption and are not substrates of P-glycoprotein. The effect on pharmacokinetic proteins such as P-glycoprotein (P-gp) and cytochromes P450 (CYP) was also evaluated by SwissADME. The main function of P-gp is to protect the central nervous system from the influence of xenobiotics so they could be excreted in some tumor cells thus leading to drug resistance. On the other hand, CYP isoenzymes are involved in the drug elimination through metabolic biotransformation. The inhibition of the isoenzymes is certainly one of the main causes of pharmacokinetic-related drug interactions leading to toxic or other side effects due to the lower rate of elimination of the drug and its accumulation in

the body. Also, most of the compounds have the ability for blood-brain barrier penetration. It could be concluded that the hydrazones from series A have good oral bioavailability based on the results of the bioavailability radar and do not meet only the values for saturation. Also, the compounds have the ability to inhibit isoenzyme CYP1A2 and P-glycoprotein, and the following compounds **5.4**, **5.7**, **5.9**, **5.13-5.15** inhibit CYP2C19, CYP2D6 and CYP3A4 enzymes. According to SwissADME tool the coefficient of skin permeability (log Kp) which is a linear correlation between the size of the molecule and the lipophilicity. The more negative the log Kp value (with Kp in $cm.s^{-1}$), the less permeable is the molecule through the skin. The ligand with the lowest permeability is **5.15** with a value of -6.06, and for the other compounds the coefficient varies from -5.17 to -6.06. According to the algorithm, values below -10 correspond to a ligand insoluble in water, between -10 and -6: slightly soluble, from -6 to -4: moderately soluble, from -4 to -2: soluble, from -2 to 0: very soluble and above 0: highly solubility. The solubility in water, which has been studied by several methods, has values from -3.59 to -4.32, i.e. hydrazones have moderate solubility.

In line with Molinspiration tool, SwissADME predicts high intestinal absorption for all compounds from series B as well as good blood-brain barrier penetration for compounds **5.16** and **5.21-5.23.** The results regarding the TPSA parameter from the program SwissADME are in good correlation with the data from Molinspiration. The SwissADME predicted values from -3.43 to -4.04 for the solubility of compounds **5.16-5.27** in water i.e. they would be soluble enough to act as orally administered pharmaceutical agents and deliver a sufficient amount of the active ingredient. The coefficient of skin permeability (log Kp) vary in the interval from -5.50 to -6.35 for the compounds from series B. The hydrazone **5.20** is the least permeable through the skin based on the lowest value -6.35. The results from the SwissADME radar of bioavailability also support that the compounds meet all requirements for drug likeness, with the sole exception of the values for saturation (carbon atoms in sp^3-hybridization). The results showed that none of the hydrazones is expected to be substrate of the P-gp protein and it would be unable to eliminate the newly synthesized hydrazones from the CNS. Most of the studied ligands are expected to inhibit the CYP1A2 isoform while compounds **5.21-5.25** and **5.27** might be inhibitors of both CYP2C19 and CYP2D6 enzymes.

The synthesized hydrazones from series C have a good intestinal absorption, and compounds **5.28** and **5.33-5.35**, according to the BOILED-Egg method, also satisfy the criteria for blood-brain barrier penetration. P-glycoprotein will not eliminate any of the newly synthesized hydrazones from the central nervous system. The bioavailability radar shows that all compounds implement the optimal properties – lipophilicity, polarity, solubility, etc. Most derivatives do not accomplish the values for saturation, except for hydrazones **5.34-5.36**, which according to the radar are the most suitable drug candidates. Compounds **5.34-5.36** inhibit all CYP enzymes included in the program (CYP1A2, CYP2C19, CYP2C9, CYP2D6, CYP3A4). The lowest skin permeation coefficient (logKp) value was -6.17 for hydrazone **5.32**. The solubility of the newly synthesized benzimidazolyl hydrazones ranges from -3.72 to -4.34, indicating that they are slightly soluble in water.

IV. Conclusions

1. A methodology was optimized for the synthesis of 1*H*-benzimidazol-2-yl hydrazones allowing the introduction of various substituents in the benzimidazole fragment and phenyl moiety. The methodology does not require specific reagents or catalysts and affords the 1*H*-benzimidazol-2-yl hydrazones in good yields. As a result, 40 1*H*-benzimidazol-2-yl hydrazones were synthesized – 37 of them are new, not described previously in the literature.
2. Based on the calculated Gibbs energies, it was established that for 1*H*-benzimidazol-2-yl hydrazones containing a hydroxyl group at *ortho* position in the phenyl moiety, the imino form is preferred, while for the rest of the hydrazones - the amino form is preferred. In the most favoutable moleculat structure tt was observed *E* configuration of the double azomethine bond and the *s-trans* conformation of the simple N-N bond.
3. Four complexes of the 1*H*-benzimidazol-2-yl hydrazones, containing hydroxy groups at the *ortho*-position in the phenyl ring, with Cu(II) and Fe(II) were synthesized. Two of the complexes are new, not described previously in the literature. The results from the physico-chemical analysis and theoretical calculations suggested that the complexes are formed by coordination of one molecule benzimidazolyl hydrazone with one metal atom.
4. The studied hydrazones exhibited a remarkable larvicidal effect on muscle larvae of *T. spiralis*, superior that of the established drugs albendazole and ivermectin, which makes them promising candidates for further research. Hydrazones containing one or more hydroxyl groups in the phenyl moiety posessed en excellent larvicidal effect. The results indicated that the presence of an OH group at 3-position in the phenyl ring is critual for masnifestation of higher anthelmintic activity. The presence of a methyl group in the benzimidazole fragment does not significantly affect the anthelmintic activity.
5. Most of the studied 1*H*-benzimidazol-2-yl hydrazones exhibited concentration-dependent cytotoxic activity towards cell lines MCF-7 and AR-230. 50% Inhibitory activity (IC_{50}) values towards the tumor cells were found at micromolar concentrations and the cytotoxicity towards the normal mouse fibroblast 3T3/CCL-1 cells was significantly lower. The results indicated that the presence of a hydroxyl group at *ortho*-position in the phenyl ring, accompanied by a hydroxyl or methoxy group at another position, as well as the presence of three methoxy groups in the phenyl ring, leads to prominent antiproliferative effect. The introduction of the methyl group at the 5(6)-position in the benzimidazole fragment is beneficial for the enhancement in the antiproliferative effect of the hydrazones containing one or two hydroxy groups. The cytotoxic activity of the studied complexes was in the low micromolar concentration range in both tumor cell models, and in addition, an increase in the activity of complex **6.1** was observed regarding the ligand **5.16.** from which it was derived.
6. The compounds modulate the *in vitro* polymerization of tubulin to varying extend, depending on their molecular structure. Most compounds prolonged the nucleation phase and slowed down the tubulin polymerization to a greater extent than nocodazole. The interactions of the investigated compounds with tubulin were clarified using molecular docking.
7. The *in vitro* evaluation of the antioxidant properties of the new 1*H*-benzimidazole-2-yl hydrazones based on the stable free radicals ABTS and DPPH as well as ferrous iron induced oxidative molecular damage in lecithin and deoxyribose, revealed that the di- and trihydroxy substituted 1*H*-benzimidazole-2-yl hydrazones were the most potent scavengers within the whole series. Their radical scavenging activity of the hydrazones is

improved compared to other benzimidazole derivatives such as N-methyl-1,3,4-thiadiazol-2-amine and 4-methyl-2H-1,2,4-triazole-3(4H)-thione moieties, 2-amino- and 5-aryl-1,3,4-oxadiazole moieties moieties and N,N-disubstituted benzimidazole-2-thione hydrazine derivatives. the observed effects of the hydroxyl substituted 1*H*-benzimidazole-2-yl hydrazones are close to those of catechin and flavonol compounds and superior to melatonin derivatives.

8. The hydrazones show versatile radical-scavenging ability – they could deactivate the free radicals •OCH_3, •OOH и •$OOCH_3$ through several mechanisms (HAT, SPLET и RAF) in polar and nonpolar medim. The transfer of a hydrogen atom or proton (the hydroxyl groups in the phenyl ring, the amino group of the hydrazone fragment) and the formation of radical adducts at different carbon atoms could be exerted by various functional groups in the molecular structure of the hydrazones.

V. Contribution

New benzimidazole derivatives - 1*H*-benzimidazol-2-yl hydrazones containing phenyl ring with halogen atoms, hydroxyl- and methoxyl groups, which exhibit combined antioxidant, antineoplastic and/or anthelmintic action, was developed. Several compounds among them were selected, which suppress the tumor cell proliferation at very low micromolar concentrations, as well as possess a remarkable larvicidal effect. By *in vitro* experiments, the putative common mechanism of antineoplastic and anthelmintic action – modulation of tubulin polymerization, has been established. The mechanisms of antioxidant activity, interaction with tubulin, drug likeness, oral bioavailability, gastrointestinal absorbtion and blood brain barrier penetration were studied by theoretical methods.

List of publications:

1 Anichina, K., Argirova, M.**,** Tzoneva, R., Uzunova, V., Mavrova, A., Vuchev, D., Popova-Daskalova, G., Fratev, F., Guncheva, M.**,** Yancheva, D. 1*H*-Benzimidazole-2-yl Hydrazones as Tubulin-targeting Agents: Synthesis, Structural Characterization, Anthelmintic activity and Antiproliferative activity against MCF-7 breast carcinoma cells and Molecular docking studies. Chemico-biological interactions, 345, Elsevier, 2021, DOI:10.1016/j.cbi.2021.109540, 109540. SJR (Scopus):0.943, JCR-IF (Web of Science):5.194; Q1, не оглавява ранглистата (Web of Science).

2 Argirova, M.**,** Georgieva, M., Hristova-Avakumova, N., Vuchev, D., Popova-Daskalova, G., Anichina, K., Yancheva, D.. New 1*H*-benzimidazole-2-yl hydrazones with combined antiparasitic and antioxidant activity. RSC Advances, 11, Royla Society of Chemistry, 2021, DOI:10.1039/D1RA07419A, 39848-39868. SJR (Scopus):0.75, JCR-IF (Web of Science):3.361; Q1, не оглавява ранглистата (Scopus).

List of citations regarding publication 1:

1. Laxmikeshav, K., Sharma, P., Palepu, M., Sharma, P., Mahale, A., George, J., Phanindranath, R., Dandekar, M.P., Kulkarni, O. P., Nagesh, N., Shankaraiah, N. “Benzimidazole based bis-carboxamide derivatives as promising cytotoxic agents: Design, synthesis, in silico and tubulin polymerization inhibition” *Journal of Molecular Structure* (2023) 1271, 134078
2. Bukhari S. N. A. , Ejaz, H. , Elsherif M.A. , Junaid K., Zaki I. , Masoud R.E. "Design and Synthesis of Some New Furan-Based Derivatives and Evaluation of In Vitro Cytotoxic Activity", *Molecules* 2022, 27(8), 2606;
3. Celik, I. , Ayhan-Kılcıgil, G. , Karayel, A. , Guven, B. ,Onay-Besikci, A. "Synthesis, molecular docking, in silico ADME, and EGFR kinase inhibitor activity studies of some new benzimidazole derivatives bearing thiosemicarbazide, triazole, and thiadiazole" *Journal of Heterocyclic Chemistry* (2022) 59 (2) 371-387
4. Putterill, B., Rono, C., Makhubela, B., Meyer, D., Gama, N. “Triazolyl Ru(II), Os(II), and Ir(III) complexes as potential HIV-1 inhibitors” *BioMetals*, (2022) 35 (4), 771-784
5. Nagesh, K.M.J., Prashanth, T., Khamees, H.A., Khanum, S.A. “Synthesis, analgesic, anti-inflammatory, COX/5-LOX inhibition, ulcerogenic evaluation, and docking study of benzimidazole bearing indole and benzophenone analogs” *Journal of Molecular Structure*, (2022) 1259, 132741

Reporting to scientific forums of scientific results on the topic of the dissertation:

- Poster presentation

1. „Synthesis, characterization and evaluation of the biological activity of new benzimidazole derivatives“ (Maria Argirova) - *European School of Medicinal Chemistry ESMEC*, гр. Урбино, Италия, 30 юни – 4 юли 2019 г.
2. „In vitro evaluation of the effect of new 1H-benzimidazolyl hydrazones derivatives on tubulin polymerization“ (Argirova M., Guncheva M., Yancheva D., Anichina K.) - *EFMC International Symposium on Advances in Synthetic and Medicinal Chemistry*, гр. Атина, Гърция, 01 – 05 септември 2019 г.
3. „Radical-scavenging activity of new benzimidazolyl hydrazones towards stable free radicals“ (Maria Argirova, Nadya Hristova-Avakumova, Denitsa Yancheva, Vera Hadjimitova) - *Third International Conference on Bio-antioxidants,* гр. Несебър, България, 17-21 септември 2019 г.
4. „Combined *in vitro* evaluation of antiparasitic and protective effect towards biologically important molecules of new 1*H*-benzimidazol-2-yl hydrazones“ (Maria Argirova, Dimitar Vuchev, Nadya Hristova-Avakumova, Kameliya Anichina, Miglena Georgieva, Denitsa Yancheva) - *Eighth international conference on radiation in various fields of research (2020)*, виртуална конференция, 20-24 юли 2020 г.
5. „Novel 2-amino-benzimidazole hydrazones as promising antiproliferative agents“ (Maria Argirova, Georgi Momekov, Maya Guncheva, Emiliya Cherneva, Kamelya Anichina, Denitsa Yancheva) -

EFMC-International symposium of medicinal chemistry and EFMC-Young medicinal chemistry symposium (2020), виртуална конференция, 9 септември 2020 г.

6. „New 2-amino benzimidazolyl hydrazone complexes: synthesis, spectroscopic and DFT investigation“ (Maria Argirova, Emiliya Cherneva, Denitsa Yancheva) - *Research Infrastructure in support of Science, Technology and Culture - Inframat*, София, 29-30 септември 2020 г.
7. „Combined evaluation of the antioxidant and anthelmintic activity of new 2-amino benzimidazolyl hydrazones“ (Maria Argirova, Petko Denev, Dimitar Vuchev, Kameliya Anichina, Denitsa Yancheva) - *European School of Medicinal Chemistry ESMEC*, виртуална конференция, 28 юни-1 юли 2021 г.
8. „Synthesis of novel 5(6)-methyl-2-amino-benzimidazolyl hydrazones as promising anticancer agents“ (Maria Argirova, Georgi Momekov, Maya Guncheva, Emiliya Cherneva, Kamelya Anichina, Denitsa Yancheva) - *8th edition of the EFMC Young Medicinal Chemists' Symposium (EFMC-YMCS)*, виртуална конференция, 9-10 септември 2021 г.
9. „Synthesis and characterization of new benzimidazole-based complexes“ (M. Argirova, S. Koleva, D. Yancheva, E. Cherneva, K. Anichina)- *XIX Научна постерна сесия за млади учени, докторанти и студенти – ХТМУ*, София, 17 юни 2022 г.
10. „New 5(6)-methyl-1*H*-benzimidazol-2-yl hydrazones: synthesis, combined evaluation of the anthelminthic and antioxidant activity and performed quantum-chemical calculations“ (M. Argirova, M. Georgieva, N.Hristova-Avakumova, D. Vuchev, K. Anichina, D. Yancheva) - *8th EuChemS Chemistry Congress (ECC8)*, Лисабон, 27 август - 01 септември 2022 г.

➢ Oral presentation

11. „Синтез и структурно охарактеризиране на нови 1*H*-бензимидазол-2-ил- хидразони“ (Мария Аргирова, Деница Янчева, Камелия Аничина) - *Дванадесети пролетен семинар „Интердисциплинарна химия*, Творчески дом – БАН, Златните мостове, София, 19 – 21 април 2019 г.
12. „Изследване на тавтомерни превръщания на 1*H*-бензимидазол-2-ил хидразони чрез ИЧ спектроскопия и DFT пресмятания“ (Мария Аргирова, Деница Янчева, Камелия Аничина) - *XVIII Национална конференция по химия за студенти и докторанти 2019* – Софийски университет, София, 15 - 17 май 2019 г.
13. „New benzimidazolyl hydrazones - synthesis and combination study of the radical-scavenging activity“ (Maria Argirova) - *Global Women's Breakfast*, София, 12 февруари 2020 г.
14. „Експериментални и теоретични изследвания на радикал-улавящата способност на 2-амино бензимидазолил хидразони“ (Мария Аргирова, Миглена Георгиева, Надя Христова-Авакумова, Камелия Аничина) - *Тринадесети пролетен семинар-уебинар "Интердисциплинарна химия"*, виртуална зала Moodle/Big Blue Button, 22–26 юни 2020 г.
15. „Нови 1*H*-бензимидазол-2-ил-хидразони с антирадикалова, антипролиферативна активност и модулиращ ефект върху полимеризацията на тубулин“ (Мария Аргирова, Георги Момеков, Надя Христова-Авакумова, Мая Гунчева, Емилия Чернева, Камелия Аничина, Деница Янчева) - *XIX Национална конференция по химия за студенти и докторанти 2021*, София, 2-4 юни 2021 г.
16. „Newly synthesized 5(6)-methyl-1*H*-benzimidazolyl hydrazones as promising antioxidant and anticancer agents“ (M. Argirova, N. Hristova-Avakumova, E. Cherneva, G. Momekov, D. Yancheva) - *XLV "A. Corbella" International Summer School on Organic Synthesis – ISOS 2021*, виртуална конференция, 14-17 юни 2021 г.
17. „New benzimidazole-based drug candidates with antineoplastic and antiparasitic activity“ (M. Argirova, G. Momekov, D. Vuchev, E. Cherneva, K. Anichina, D. Yancheva) - *Трети интердисциплинарен докторантски форум*, Кюстендил, 05-08 юни 2022 г.

Acknowledgments:

This work has been financially supported by the National Science Fund of Bulgaria, Contract КП-06-Н39/4.